Nonstationary Shear-Wave Velocity Randomization Approach to Propagate Small-Scale Spatial Shear-Wave Velocity Heterogeneities into Seismic Response

Eliane Youssef, Cécile Cornou, Dalia Youssef Abdel Massih, Tamara Al-Bittar

Nonstationary Shear-Wave Velocity Randomization Approach to Propagate Small-Scale Spatial Shear-Wave Velocity Heterogeneities into Seismic Response

Eliane Youssef[1*], Cécile Cornou[2], Dalia Youssef Abdel Massih[3] and Tamara Al-Bittar[4]

[1] PhD, Univ. Grenoble Alpes, Univ. Savoie Mont Blanc, CNRS, IRD, Univ. Gustave Eiffel, ISTerre, 38000 Grenoble, France. Faculty of Engineering, Lebanese University, Hadath, Baabda, Lebanon. ORCID: https://orcid.org/0000-0001-6138-013X.

*Corresponding author. e-mail: eliane.youssef@univ-grenoble-alpes.fr ; eliane-youssef@hotmail.com

[2] Research director, Univ. Grenoble Alpes, Univ. Savoie Mont Blanc, CNRS, IRD, Univ. Gustave Eiffel, ISTerre, 38000 Grenoble, France.
e-mail: cecile.cornou@univ-grenoble-alpes.fr

[3] Professor, Faculty of Engineering, Lebanese University, Roumieh, Mount Lebanon, Lebanon.
ORCID: https://orcid.org/0000-0002-5144-8337
e-mail: dalia.abdelmassih@ul.edu.lb

[4] Professor, Faculty of Engineering, Lebanese University, Ras-Maska, President Michel Sleiman Campus, Lebanon. ORCID: https://orcid.org/0000-0002-3382-7069
e-mail: Tamara.albittar@gmail.com

(Accepted version for publication in the Journal of Geotechnical and Geoenvironmental Engineering, © ASCE, ISSN 1090-0241)

Cite as: Youssef, E., Cornou, C., Youssef Abdel Massih, D., Al-Bittar, T. 2024. Non-stationary shear-wave velocity randomization approach to propagate small-scale spatial shear-wave velocity heterogeneities into seismic response. J Geotech Geoenviron Eng; 150(10):04024102. https://doi.org/10.1061/JGGEFK.GTENG-11884.

Nonstationary Shear-Wave Velocity Randomization Approach to Propagate Small-Scale Spatial Shear-Wave Velocity Heterogeneities into Seismic Response

Eliane Youssef[1*], Cécile Cornou[2], Dalia Youssef Abdel Massih[3] and Tamara Al-Bittar[4]

Abstract. Recent studies in earthquake engineering have outlined the difficulty of ground response analyses (GRAs) to replicate the observed ground motion and related variability at borehole array sites. Improvement of the seismic site response estimation requires accounting for and propagating the uncertainties in local soil conditions into surface ground motion. Uncertainties in site conditions arise from a number of factors, among which the uncertainties in the shear-wave velocity (V_S) that are mainly caused by the natural spatial variability of soils and rocks.

In this paper, a novel V_S randomization approach is proposed to propagate the small-scale spatial V_S heterogeneities into samples of V_S profiles within a non-stationary probabilistic framework, to be further used in 1-dimensional (1D) GRAs. The non-stationary approach is based on partitioning a borehole base-case V_S profile into several locally stationary layers. The proposed approach was applied at three European sites exhibiting different subsurface soil conditions. Compared with both the classical stationary and an approach from the literature for V_S randomization, the proposed approach provides a set of V_S profiles fully consistent with the pseudo-experimental site signatures in terms of surface-wave dispersion curves, fundamental and higher mode resonance frequencies and site amplification. This paper also outlines the importance of the method used to measure V_S profile in both the estimation of depth-dependent variability of V_S at a given site and the prediction of site response variability. DOI: 10.1061/JGGEFK.GTENG-11884.

Keywords: geotechnical earthquake engineering, spatial variability, uncertainty, seismic site response, shear-wave velocity randomization, random fields.

Introduction

In geotechnical earthquake engineering, seismic site response analysis has become an essential requirement to quantify the seismic hazard level and the associated damage for most projects, particularly those dealing with critical facilities and high-priority lifelines. In a typical scenario, the prediction of the one-dimensional (1D) seismic site response consists of vertically propagating the seismic shear waves through horizontally stacked and laterally infinite homogeneous soil layers until reaching the soil surface (Kramer 1996). Despite the wide application of this approach to estimate the surface ground motion, still, numerous studies confirmed that the predicted site response rarely matches the recorded ground motion at most borehole array sites (e.g., Thompson et al. 2012; Kaklamanos and Bradley 2018; Laurendeau et al. 2018; Pilz and Cotton 2019; Tao and Rathje 2020). The main limitations in this deterministic prediction lie in assuming 1D wave propagation together with over-simplification of the dynamic soil properties that do not allow the full complexity of the seismic wavefield (diffracted body and surface waves, seismic waves mode conversion, scattering, etc.) to be simulated (Thompson et al. 2009; Li and Assimaki 2010; Zalachoris and Rathje 2015; Kaklamanos and Bradley 2018). In reality, our knowledge of the vertical and horizontal spatial soil heterogeneities at the local scale (from a couple to tens of meters) is very limited. Failing to carefully account for the soil spatial heterogeneities will highly limit the effectiveness of any 1D, 2D, or 3D ground motion simulation to reproduce surface ground motion characteristics (e.g. among others, Nour et al. 2003; Thompson et al. 2009; Li and Assimaki 2010; Rathje et al. 2010; Pagliaroli et al., 2014; Parolai et al. 2015; Pilz and Fäh 2017; El Haber et al. 2019; Tao and Rathje 2019; De Martin et al. 2021; Tchawe et al. 2021; De la Torre et al. 2022; Hallo et al. 2022).

In site response estimation, uncertainties arising from soil conditions are usually classified into two main categories: epistemic uncertainty and aleatory variability. Epistemic uncertainties result from the lack of sufficient knowledge and measurement errors while aleatory variabilities are the inherent variability of soil properties that are caused by natural and complex geological phenomena (e.g., erosion, sedimentation, deposition…) and other environmental processes and anthropogenic activities

(e.g., urban development, landfilling…) (Phoon and Kulhawy 1999 a&b; Einsele 2000). Uncertainties in the description of site conditions exist in characterizing the geometrical site properties (i.e., geologic and topographic configurations, sediment-bedrock depth) and the dynamic site properties (i.e., shear-wave velocity (V_S), shear modulus reduction, attenuation). The estimation of these properties and particularly V_S is highly affected by the natural spatial variability of soils, manifested through multiple-scale stratigraphic heterogeneities of V_S structure. A realistic representation of V_S, along with its variability, is thus a primary ingredient in any 1D, 2D, and 3D Ground Response Analysis (GRA) model. This is only feasible through a proper quantification of V_S variability and its propagation into samples of V_S profiles that are capable of reflecting the true soil behavior with uncertainty consideration. Derivation of the V_S profile in near-surface geological materials is typically carried out through invasive borehole measurement methods (e.g., Down-Hole, Cross-Hole) or active and passive non-invasive surface-wave methods (e.g., Socco and Strobbia 2004; Foti et al. 2018). For any performed measurement technique, invasive or not, the estimation of V_S is influenced by epistemic uncertainties and aleatory variabilities that control the heterogeneities in the experimental data and the degree of variability expected at a given site (Baise et al. 2011; Thompson et al. 2012).

Accounting for the variability of V_S in 1D site response, is usually done through V_S heterogeneities propagated into random samples of V_S profiles. These samples are subsequently used to perform several 1D GRAs to replicate the effect of the velocity variability in the average site response prediction and related variability. Toro (1995) used an extensive V_S database to construct generic and site-specific V_S randomization models, provided a generic site classification, and a base-case V_S profile. This approach was broadly used throughout the years, mainly to investigate the effect of V_S uncertainty on ground motion variability (among others, Li and Assimaki 2010; Rathje et al. 2010; Rodriguez-Marek et al. 2014). However, such an approach does not necessarily guarantee the experimental site signatures in terms of surface-wave dispersion curves and fundamental resonance frequency (f_0) to be replicated, as recently investigated (Griffiths et al. 2016a&b; Teague et al. 2018), which can potentially lead to excessive variability of V_S and an overestimation of the expected variability in site response estimates

(Teague et al. 2018; Kaklamanos et al. 2020). Passeri et al. (2020) then proposed to randomize the cumulative S-wave travel times instead of interval V_S profiles to reduce the variability in the generated V_S samples of the Toro (1995) approach. The authors calibrated the model from a large database of surface-wave measurements. The application of this approach at the Mirandola site in Italy provided good agreement with the experimental site signatures, although very low levels of variability were obtained (Passeri et al. 2020; Toro 2022). Toro (2022) argued that the uncertainties in surface-wave methods implemented in such V_S randomization approaches (e.g., Teague et al. 2018; Passeri et al. 2020) are controlled by the uncertainty in the dispersion curves that is assumed to encompass both epistemic uncertainties and aleatory site variabilities. As such, the uncertainty from the non-uniqueness of surface-wave inversion should be carefully treated to avoid an underestimation of the site response variability (Toro 2022). Hallal et al. (2022a) further demonstrated that an increase in the variability level in Passeri et al. (2020) is required to appropriately model subsurface V_S variability and provided guidelines for improved implementation of the travel-time randomization (e.g., bounding layers thicknesses). Toro (2022) also proposed to handle the variability in V_S as depth-dependent (i.e., decreasing with depth) based on recent findings (Garofalo et al. 2016a&b; Shi and Assimaki 2018; Passeri et al. 2020) contrarily to the initial proposition in Toro (1995).

Although the search for reliable and robust V_S randomization approaches has rapidly increased in recent years (Passeri et al. 2020; Hallal et al. 2021; Vantassel and Cox 2021), most of the existing techniques that intend to account for subsurface spatial variability in 1D GRAs have not been thoroughly benchmarked at downhole array sites, despite some recent comparison between randomization approaches and recorded ground motion (Teague et al. 2018; Kaklamanos et al. 2020; Hallal et al. 2022b).

Regardless of the diversity of randomization approaches, the separation between what constitutes epistemic uncertainties and aleatory variabilities is often overlooked. The spatial heterogeneities in V_S structure are the result of natural and complex geological processes, thereby they display variable and aleatory properties. In this paper, we focus on this aleatory aspect manifested through the small-scale

(few decimeters to tens of meters) spatial heterogeneities of V_S. Random variables and random fields (RFs) were extensively used in literature to represent small-scale spatial heterogeneities in soil properties (e.g., Popescu 1995; Fenton 1999; Phoon and Kulhawy 1999a&b; Griffiths et al. 2009; Soubra and Youssef Abdel Massih 2009; Al-Bittar and Soubra 2013). More recently, RFs were used to incorporate the spatial heterogeneity of V_S in site response estimation (Thompson et al. 2009; Pagliaroli et al. 2014; El Haber et al. 2019; Tchawe et al. 2021).

To build a probabilistic model for V_S, the RF is defined by a Probability Density Function (PDF) and an Auto-Correlation Function (ACF). In a classical RF theory, the statistical modeling of the spatial variability strongly depends on the stationarity of the data collected (Jaksa 1995). Stationarity of a RF is guaranteed when the mean and variance of its PDF are constant and the ACF depends only on the lag distance between two locations (Vanmarcke 1983). Otherwise, the RF is considered to be non-stationary or statistically heterogeneous. Soil properties are in general non-stationary as a result of strong geomorphological processes and the increase in confining pressure exerted by the soil mass with increasing depth (Einsele 2000). The non-stationarity is further increased by the irregularity of the stresses applied on the soil surface and built up by the different deposition conditions (Chenari and Farahbakhsh 2015). Therefore, a realistic representation of soil properties must account for their non-stationary state, contrary to what was often assumed (e. g., Youssef Abdel Massih 2007; Salloum 2015; El Haber et al. 2019).

Over the past years, the non-stationarity of material properties has gained a lot of attention particularly in geostatistical and environmental studies (e.g., Kleiber 2016; Montoya-Noguera et al. 2019) and in geotechnical engineering applications (e.g., Chenari and Farahbakhsh 2015; Chenari et al. 2018; Jiang and Huang 2018). In these approaches, non-stationarity is typically modeled by multiplying a varying standard deviation or variance function by a stationary correlation function. Dividing the random process into multiple stationary processes with distinct variance values, allows the process to adapt to highly variable material properties. The technique of model decomposition has allowed to

transform the non-stationary RF into multiple locally stationary RFs which achieves a more realistic representation of material properties.

The main objective of this work is to properly incorporate the aleatory variability of V_S into 1D GRAs through a robust yet simple approach that accounts for the non-stationary spatial heterogeneity of V_S and propagates it into representative samples of V_S profiles. The set of randomized V_S profiles can then be used to perform numerous 1D GRAs to obtain an averaged site response.

This article starts by introducing the proposed V_S randomization approach, employing a non-stationary probabilistic method to account for the vertical spatial variability of V_S structure. Following the methodology, we extensively apply the proposed approach to three European sites as part of the InterPACIFIC project (Garofalo et al. 2016b). The application presents site response characteristics, in terms of site signatures (dispersion curves, resonance frequencies), as well as site amplification obtained using the proposed approach. To evaluate modeling accuracy, the results are compared with those obtained from both the classical stationary RF approach and the Toro (1995) approach, assessing compatibility with several pseudo-experimental site signatures.

A non-stationary probabilistic approach for V_S randomization

In a probabilistic model, the RF is defined by the PDF and the ACF, as stated previously. The PDF of V_S describes the distribution of V_S data and is defined by a mean value μ_{Vs} and a standard deviation σ_{Vs}. Here, the ACF gives the values of the correlation function between two arbitrary points at two different locations and is completely characterized by the so-called 'scale of fluctuation'. The scale of fluctuation denoted θ is an indicator of the distance within which values of V_S are still correlated. Once the RF parameters are quantified, one needs to discretize the RF into a finite set of RVs. After the discretization step, realizations of the RF may be performed by randomly generating a prescribed number of samples (e.g., Al-Bittar et al. 2018; El Haber et al. 2019).

To properly propagate the spatial variability of V_S, the non-stationarity in the RF statistical parameters should be properly considered. For this purpose, the stationary RF approach was re-

formulated in this study to account for the variability of the V_S mean and variance with depth. The variability in μ_{Vs} and σ_{Vs} was introduced through a layering scheme of the original V_S profile. In this paper, the layering followed the interfaces between the geological formations and was performed by adding a new layer at each interface to allow a proper tracking of the vertical spatial variability of V_S. The selection of the layer thickness is thus controlled by the stratification of the soil deposits while the number of layers is related to the level of the lithological heterogeneity expected at the site. This allowed the V_S data in each layer to be treated as stationary locally. Consequently, the non-stationarity of the RF was modeled through multiple small-scale stationary RFs. Each small-scale RF was individually quantified and then discretized to estimate V_S values at each depth. In the next subsections, the quantification of V_S variability and the RF discretization are presented.

Quantification of the V_S random field

The quantification of the spatial variability of V_S was performed as follows (Popescu 1995):

(1) Visually check the available V_S data for each layer to remove spurious measurements. A re-sampling was required in some cases to achieve a constant step throughout the depth of the profile;

(2) Check for the presence of a trend in the data (e.g., linear, quadratic). In case a trend is identified, apply a detrending process to the measured values. Subsequently, perform a normalization procedure by dividing the detrended values by the layer σ_{Vs}. This results in achieving a zero μ and unit σ random process, providing a stationary and homogeneous dataset;

(3) Compute the ACF defined between two values of V_{Si} measured at z_i and distanced by a lag τ as in Eq.1:

$$\rho_\tau = \frac{\sum_{i=1}^{n-\tau}\left(V_{S_i} - \mu_{V_S}\right)\left(V_{S_{i+\tau}} - \mu_{V_S}\right)}{\sum_{i=1}^{n}\left(V_{S_i} - \mu_{V_S}\right)^2} \quad , \quad \tau = 0,1,2,\dots,n-1 \tag{1}$$

Where n is the number of data measurements in a layer, τ is the lag distance between V_{Si} and $V_{Si+\tau}$ measured at locations z_i and $z_{i+\tau}$, respectively, and μ_{Vs} is the mean value of V_S.

Next, the ACF was determined by fitting the obtained experimental curve to theoretical existing ACF functions. The best-fitted ACF was selected based on the lowest root-mean-square error (R^2) and the scale of fluctuation of V_S, θ, was determined using the parameters of the fitted ACF.

(4) Find the PDF of V_S and its statistical parameters: μ_{Vs}, σ_{Vs}, and a coefficient of variation $CoV_{Vs} = \sigma_{Vs} / \mu_{Vs}$ that quantifies the range of dispersion of the data around its mean. The term σ_{Vs} is used to define the standard deviation of V_S data, whereas σ_{lnVs} particularly stands for the standard deviation of log-normally distributed V_S data. To avoid any confusion with σ_{Vs}, the CoV_{Vs} representing the percentage of V_S variability, is typically used here, allowing an easier interpretation of the variability degree.

Once V_S variability was quantified, the resulting PDF and ACF parameters were subsequently used to discretize the RF of V_S, referred to as RF(V_S) hereafter.

Discretization of the V_S random field

For computational purposes, the RF has to be expressed using a finite number of RVs. This step is referred to as RF discretization. Various methods for RF discretization have been published in the literature, a comprehensive overview of such methods is given in Sudret and Der Kiureghian (2000). The efficiency of a method depends on its ability to approximate the original RF accurately with a minimum number of RVs. The Expansion Optimal Linear Estimation method (EOLE) which is part of the series expansion methods was used herein since it provides a minimum value for the variance of the error using an optimal number of RVs (Li and Der Kiureghian 1993). In this method, a stochastic mesh was first defined, and then the auto-correlation matrix $\Sigma_{\chi;\chi}$ was computed using the fitted ACF. To estimate the RF(Vs) at any location z, the EOLE method makes use of the statistical parameters μ_{Vs} and σ_{Vs} as well as the fitted ACF as follows:

$$\tilde{V}_S(z) = \mu_{V_S} + \sigma_{V_S} \sum_{i=1}^{N} \left(\frac{\xi_i}{\sqrt{\lambda_i}} (\Phi_i)^T \sum_{V_S(z);\chi} \right), \quad i = 1, \dots, N \tag{2}$$

In Eq. (2), $\widetilde{V_S}$(z) is the approximation of RF(Vs), ξ_i is the vector containing independent standard normal RVs, λ_i and Φ_i are the eigenvalues and eigenvectors, respectively, of the auto-correlation matrix $\Sigma_{\chi;\chi}$ and

$\Sigma_{V_S(z);\chi}$ represents the correlation vector between the RF(V_S) at the grid points of the stochastic mesh and the RF at the arbitrary point z. The series of Eq. (2) was truncated to a number of terms N (expansion order), which is smaller than the number of grid points, after sorting the eigenvalues in descending order. This number N should ensure that the variance of the error is smaller than a prescribed threshold (between 5 to 10%). The variance of the error on the random field in the EOLE method is given by Eq. 3:

$$Var\left[V_S(z) - \widetilde{V}_S(z)\right] = \sigma_{V_S}^2 - \sum_{i=1}^{N} \frac{1}{\lambda_i} \left((\Phi_i)^T \sum_{V_S(z);\chi} \right)^2 \quad (3)$$

$V_S(z)$ and $\widetilde{V_S}(z)$ are the exact and approximate values of the RF(V_S) at a given location z. Additional details about the EOLE formulation can be found in Peng et al. (2022). A detailed representation of the methodology used to quantify and discretize the RF(V_S) is schematized in Figure 1. All the RF quantification and discretization codes used in this paper are equally provided in a GitLab repository with detailed commentary indicated in the Data Availability Statement.

Application to the InterPACIFIC project sites

This section presents the application of the proposed non-stationary RF approach to the InterPACIFIC project sites. After presenting the three sites, the results of V_S variability quantification and a description of the RF(V_S) discretization are provided.

Presentation of sites

The borehole geological and geophysical data used in this study were collected within the framework of the InterPACIFIC project (Intercomparison of methods for site parameter and velocity profile characterization) (Garofalo et al. 2016a&b). The investigated sites exhibit different subsoil conditions: soft soil, stiff soil, and hard rock. At each site, several V_S profiles derived from invasive measurements (Cross-Hole, Down-Hole, and P (compression) - S (shear) wave logging§) are available.

The first test site is located in Mirandola, Italy on the Po River plain. The boreholes drilled at this location revealed a soft alluvial soil overlaying a Pleistocene substratum at 112 meters depth. The alluvial deposits are composed of alternating layers of sand and silt clay. The in-hole measurements indicated a stiffer layer between 50 m and 150 m depth. The second site is located in the Grenoble's alpine valley (France), in the French Alps. It consists mainly of very deep and stiff alluvial deposits composed of a few tens of meters of sand and gravel followed by soft clay that overlay deeper Quaternary lacustrine layers of clay and marl. The bedrock is reached at depths between 500 and 800 meters. The third site is located in Cadarache, South-East of France, on Cretaceous outcropping limestone with thin inter-layers of marl and grey up to 50 meters depth. The stratigraphic formations from the borehole logs for the three sites are presented in Figure 2.

Application of the non-stationary probabilistic approach

From the invasive measurements conducted at each site, six V_S profiles were extracted at each site following three different in-hole methods: two Down-Hole (DH, namely DH-NS and DH-EW), two Cross-Hole (CH, namely CH1 and CH2), and two P-S suspension logging (PS-SL, namely PS-SL S-R1 and PS-SL R1-R2) V_S profiles. Figure 3 displays the six V_S profiles at each site. It's important to note that the majority of borehole measurements reached depths of approximately 112 m, 45 m, and 31 m in Mirandola, Grenoble, and Cadarache, respectively. Hence, in this study, an imposed seismic bedrock depth was fixed at each site following these borehole depths, leading to a fundamental resonance frequency of 0.7 to 0.8 Hz, 1.7 to 1.8 Hz, and around 20 Hz for Mirandola, Grenoble, and Cadarache, respectively.

For the application of the proposed non-stationary RF approach, the first step required the investigation of stratigraphic logs to define the depths of interfaces between consecutive geological formations (Figure 2). Each V_S profile was then individually layered following these interfaces, which led to 10 identified V_S layers in Mirandola, while a total of 8 layers and 4 layers were identified in Grenoble and Cadarache, respectively.

Quantification of the V_S random field

For all of the 18 V_S profiles across the three sites, the variability in each layer was quantified according to the steps presented in Section **Quantification of the Vs Random Field**. In each layer, V_S data were found to be log-normally distributed and their ACF was best fitted to an exponentially decaying function. Results of V_S quantification, notably the CoV_{Vs}, and θ, are presented in Tables 1 and 2 for Mirandola and in Tables S1, S2, S4 and S5 of Appendices S2 and S3 for Grenoble and Cadarache, respectively. The number of measured V_S samples used to compute the CoV_{Vs} and θ values for each layer depends on the layer thickness and the V_S profile measurement method. The number of V_S samples is indicated for each layer and each measurement method in Table 2 for Mirandola and in Tables S2 and S5 of Appendices S2 and S3 for Grenoble and Cadarache, respectively. Average and standard deviation values for CoV_{Vs} and θ across the six V_S profiles were also computed for each layer in each site. At all sites whatever the base-case profile, the CoV_{Vs} values exhibit a high variability between the various layers. For instance, in Mirandola the CoV_{Vs} range between 0.01% to nearly 28% for DH-EW. For all sites, the largest CoV_{Vs} are generally found in PS-SL V_S profiles since this measurement method provides a higher vertical resolution compared to DH and CH measurements. Note here that a resampling was performed on DH V_S profiles across the three sites to achieve a constant V_S data step, which led to reduced values of DH CoV_{Vs}, between 0.6% to 4.2%, on average. For a given layer, the difference in the CoV_{Vs} measured using different in-hole methods is highlighted in $CoV_{(CoV)}$. Whatever the site, the large $CoV_{(CoV)}$ values (that range from about 10-20% to about 90-130%) clearly outline that the quantification of V_S variability is strongly influenced by the investigation technique. Although θ values are also found to vary between different layers for a given borehole and between base-case profiles for a given layer, they are more consistent for most of the layers across all the study sites (Table 1 for Mirandola and Tables S1 and S4 in Appendices S2 and S3 for Grenoble and Cadarache, respectively).

Discretization of the V_S random field

Using the quantification parameters from each layer, the RF(V_S) was then generated for each layer separately across all six base-case profiles for the three sites. For the sake of simplicity, a fixed value of 2 m for θ was assumed for all layers regardless of the base-case profile. This value reflects common vertical correlation distances in soil properties (e.g., Phoon and Kulhawy 1999a&b; El Haber et al. 2019; Tchawe et al. 2021) and is in accordance with the mean θ (1.4 m ± 1.1 m) obtained after averaging all θ values across all sites. A total number of 200 realizations of RFs were generated in each layer of the six profiles and the set of randomized layers were merged to obtain the complete 200 realizations of V_S profiles relative to each base-case profile. The sufficiency of the number of realizations was checked through the convergence of μ_{Vs} and σ_{Vs} estimators using Haldar and Babu (2008) criteria with a 5% convergence rate at all depths. A convergence rate of 5% was reached after 10 to 15 realizations at all depths of the six tests and three sites. The number of 200 realizations has led to a maximum convergence of approximately 1.5% across all cases. Figure 4 shows the 200 sets of randomized V_S profiles for Mirandola together with the average V_S profiles for three of the six investigated profiles. The remaining three base-case profiles at Mirandola are presented in Figure S1 of Appendix S1. The range of V_S values in each layer is directly associated with the CoV_{Vs} of the layer (Table 2). A high CoV_{Vs} such as the case of layer number 8 of the PS-SL S-R1 test (CoV_{Vs} = 37.7%) leads to a high variability in V_S, while lower CoV_{Vs} in layers number 7 and 10 in the DH-EW test lead to an almost negligible variability. Values of CoV_{Vs} across the three sites are compatible with typical values found in the literature (Garofalo et al. 2016a; Shi and Assimaki 2018; Toro 2022). This level of vertical V_S variability is expected to be more pronounced than the lateral variability due to deposition conditions on the soil surface (DeGroot 1996; Phoon and Kulhawy 1996; Assimaki et al. 2003). For Grenoble and Cadarache, the randomized V_S profiles are illustrated in Figures S4 and S8 of Appendices S2 and S3, respectively. For the sake of clarity in the following, only results for the three base-case profiles from Mirandola (Figure 4) will be presented in the body of this paper. However, results and

figures for the other base-case profiles in Mirandola and the six base-case profiles of Grenoble and Cadarache each are provided in Appendices S1, S2, and S3, respectively.

Implementation of other existing randomization methods

For the purpose of evaluating the efficiency of the proposed Non-Stationary approach, both the Toro (1995) V_S randomization approach and the classical stationary RF approach were also applied to V_S data from the InterPACIFIC project sites. The Toro (1995) approach operates on three main schemes: (1) the layering model, which defines the thicknesses and interfaces of the layers, (2) the velocity model, which indicates V_S values at the mid-layers and (3) the depth-to-bedrock model which randomizes the bedrock depth and velocity. For the application of the Toro (1995) approach, the generic model parameters based on seismic site classification were used in this study as commonly adopted in practice in conjunction with σ_{lnVs} values proposed by Stewart et al. (2014) using the site-specific database of Toro (1995). Such σ_{lnVs} values were also used in previous studies proposing methods to propagate *Vs* uncertainties in site response (e.g. Rathje et al. 2010; Teague et al. 2018; Passeri et al. 2020). Table 3 provides the parameters used for the application of the Toro (1995) approach. The σ_{lnVs} are in the range of σ_{lnVs} inferred from individual V_S layers used for the Non-Stationary application that vary from 0.02 (CoV_{Vs} ~1%) up to 0.18 (CoV_{Vs} ~40%). The randomization was performed for all base-case profiles in the three sites using the Toro (1995) procedure implemented into STRATA Version 0.8.0 (Kottke and Rathje 2009).

For the application of the stationary approach, V_S variability was quantified using the borehole data from the soil surface till the bedrock interface as a single data set. Hence, single values for μ_{Vs} and CoV_{Vs} as well as θ were computed for each base-case profile and used for the discretization of RF(V_S). These parameters are provided in Table S7 of Appendix S4. Using the quantification results, the discretization of RF(V_S) was then performed in the same manner as the Non-Stationary approach using the EOLE method and, 200 realizations were generated around each base-case profile.

Performance of the V_S randomization approaches to predict site response

To evaluate the compatibility of randomized V_S profiles with the pseudo-experimental site signatures derived from borehole data, the theoretical dispersion curves (TDCs) and the theoretical transfer functions (TTFs) for vertically incident horizontal shear (SH) plane waves (Kennet 1983) were computed up to 20 Hz using the non-stationary, stationary and the Toro (1995) approaches. For these computations, P-wave velocities (V_P) in the sediments were randomized following a fixed dependence on randomized V_S profiles constrained by the measured Poisson's ratios in boreholes (Garofalo et al. 2016b). Accordingly, V_P values were computed using factors of 4.2, 3.5, and 1.9 with respect to V_S for Mirandola, Grenoble, and Cadarache, respectively. Bedrock velocities were fixed according to values indicated in Table 3. Mass densities in sediments were fixed at 1800 kg/m^3 in both Mirandola and Grenoble and at 2200 kg/m^3 in Cadarache while a mass density of 2500 kg/m^3 was assigned for the half-space seismic bedrock in all three sites. These assumptions are consistent with the experimental data extracted from the results of the InterPACIFIC project (Garofalo et al. 2016b). Quality factors for P and S waves were assumed to be equal to 50 and 25 in sediments and 200 and 100 in bedrock. The dispersion curves were computed using the software Geopsy Version 2.0.4 (Wathelet et al. 2020).

Dispersion curves

The TDCs relative to the sets of generated V_S profiles were compared to the dispersion curves computed from the base-case borehole data, referred to as pseudo-EDCs. For all sets of V_S profiles, the TDCs were computed for the fundamental mode of the Rayleigh wave and the mean TDCs were obtained after averaging the slowness values. The TDCs are represented in Figure 5 for three profiles in Mirandola (in Appendix S1 (Figure S2) for the other three profiles) and in Figures S5 and S9 of Appendices S2 and S3 for Grenoble and Cadarache, respectively, altogether with the pseudo-EDCs. The mean TDCs from nonstationary randomized profiles are most consistent with the pseudo-EDCs over all base-case profiles (Figures 5 (a-c); S2 (a-c); and S9 (a-c)). In Mirandola, TDCs from Stationary randomized profiles are far from reproducing the pseudo-EDCs, particularly at frequencies above 2 Hz

(Figure 5 (d) to (f) and Appendix S1, Figure S2 (d) to (f)), while the Toro (1995) mean randomized TDCs relatively succeed in reproducing the pseudo-EDCs (Figure 5 (g) to (i) and Appendix S1, Figure S2 (g) to (i)). In terms of dispersion of TDCs, individual TDCs from the Non-Stationary approach exhibit the lowest variation around the pseudo-EDCs while the ones based on the Toro approach are highly scattered around the pseudo-EDCs (Figure 5 and Appendix S1, Figure S2). TDCs inferred from the Non-Stationary and Toro approaches at Grenoble and Cadarache sites exhibit similar behavior (Figures S5 (a) to (c) and (g) to (i); and S9 (a) to (c) and (g) to (i) in Appendices S2 and S3 for Grenoble and Cadarache, respectively). At these sites however, the Stationary approach performs well in generating randomized V_S profiles with corresponding mean TDCs close to the pseudo-EDCs (Figures S5 (d) to (f); and S9 (d) to (f) in Appendices S2 and S3 for Grenoble and Cadarache, respectively), as a consequence of V_S base-case profiles not exhibiting significant increase of V_S within each layer (Figures S4 and S8 in Appendices S2 and S3 for Grenoble and Cadarache, respectively).

To assess the goodness-of-fit between TDCs and pseudo-EDCs for each realization of a V_S profile, the classical dispersion misfit (m_d) was computed as in Eq. (4) following Wathelet et al. (2004).

$$m_d = \sqrt{\sum_{i=1}^{n_f} \frac{(x_{di} - x_{ci})^2}{\sigma_i^2 n_f}} \tag{4}$$

In which, x_{di} is the pseudo-experimental phase velocity at frequency f_i, x_{ci} is the calculated theoretical phase velocity at the same frequency f_i, σ_i represents the standard deviation of the experimental data at frequency f_i when available and n_f corresponds to the number of frequency samples.

A typical m_d value below 1 indicates that the TDC falls inside the 1σ from the pseudo-EDC over the frequency range of interest. The m_d were computed for each 200-set of V_S profiles generated from the Non-Stationary, Stationary and Toro approaches and then averaged. Average m_d values are presented in Figure 6 (a) for the six profiles in Mirandola whereas m_d are presented in Figures S6 (a)

and S10 (a) of Appendices S2 and S3 for Grenoble and Cadarache, respectively. Across the three sites whatever the base-case profiles, the Non-Stationary approach succeeds in replicating the pseudo-EDCs, providing a better fit in terms of m_d values than the randomized V_S profiles from the classical stationary and the Toro (1995) approaches. Consistently with TDCs indicated in Figure 5, Toro randomized V_S profiles perform better than the V_S profiles from the Stationary approach in Mirandola but not in Grenoble and Cadarache. In addition, the coefficient of variation of phase velocities $CoV_{(Vr)}$ was computed between each 200-set of TDCs for all the profiles to evaluate the degree of variability between sets of randomized TDCs and therefore the level of ergodicity for the adopted randomization approach. Ergodicity conveys that the observation of a single realization of the RF can provide a strong indication of the probabilistic properties of that RF, i.e. the ability of each random V_S realization to be representative of the base-case profile. $CoV_{(Vr)}$ values as a function of frequency shown in Figure 6 (b) for Mirandola reach up to 9 % for the TDCs derived from the Non-Stationary approach, while higher maximum values of 22% and 34% were obtained for the TDCs using the Stationary and Toro approaches. Interestingly, high $CoV_{(Vr)}$ are observed close to the resonance frequency of the site. Similar results were obtained for Grenoble and Cadarache with significantly lower $CoV_{(Vr)}$ for Cadarache (Figures S6 (b) and S10 (b) in Appendices S2 and S3 for Grenoble and Cadarache, respectively). Across the three sites, the Non-Stationary approach thus resulted in the lowest $CoV_{(Vr)}$ (< 10% over the whole frequency range) when compared to the other two approaches confirming a high ergodicity property of the proposed V_S randomization and a best performance to replicate the pseudo-EDCs. This highlights that the generated V_S profiles succeed in reflecting the original V_S statistical properties, therefore, no posterior selection is required to screen V_S realizations that fail to reproduce the site signature, as often recommended (Teague and Cox 2016; Teague et al. 2018).

1D site amplification

The theoretical transfer functions (TTFs) were computed for the 200-set realizations of V_S profiles derived from the Non-Stationary, Stationary, and Toro approaches. The TTFs computed from borehole

data, referred to as pseudo-ETFs, were used to evaluate the accuracy of TTFs in replicating both the amplification and resonance frequencies. Figure 7 displays TTFs for three base-case profiles in Mirandola. The other three profiles are shown in Appendix S1 (Figure S3) and in Figures S7 and S11 of Appendices S2 and S3 for Grenoble and Cadarache, respectively. From a visual inspection, the TTFs related to the V_S profiles derived from the Non-Stationary approach nicely match both amplification and resonance frequency peaks within a wide range of frequencies at Mirandola and Grenoble. Although individual TTFs derived from the Toro approach are highly scattered (Figure 7 (g) to (i) and Figure S3 (g) to (i) in Appendix S1 for Mirandola and Figure S7 (g) to (i) in Appendix S2 for Grenoble), the average TTFs reproduce well the fundamental and first resonance frequency peaks at Mirandola and Grenoble. However, the highly scattered TTFs result in lower average amplification compared to the pseudo-ETFs at the first two resonance modes and an overall attenuation of average amplification at higher frequencies, as frequently observed (Thompson et al. 2009, 2012; Zalachoris and Rathje 2015; Kaklamanos and Bradley 2018; Hallo et al. 2022). Similarly to the Toro approach, TTFs derived from the Stationary approach were also very scattered leading to attenuated average amplification at high frequencies at Mirandola and Grenoble, while the average amplifications at the two first resonance modes were consistent with the pseudo-ETFs. However, the predicted average frequencies were shifted towards lower frequencies at the two first modes of resonance, in particular at the Mirandola site (Figure 7 (d) to (f) and Figure S3 (d) to (f) in Appendix S1). Such resonance frequency shift was already observed in previous studies using stationary RFs and was mainly attributed to the inability of all randomized V_S to reproduce the average S-wave cumulative travel time from the bedrock to the surface (e.g., Nour et al. 2003; El Haber et al. 2019). This behavior explains the failure of the TDCs to reproduce the pseudo-EDCs (Figure 5 (d) to (f) and Figure S2 (d) to (f) in Appendix S1 for the Mirandola site). For the Cadarache site, TTFs derived from Non-Stationary, Stationary, and Toro approaches were not fully interpretable within the frequency range of interest (up to 20 Hz) since pseudo-ETFs exhibited resonance frequencies above 20 Hz.

To quantify the goodness-of-fit between the sets of 200 TTFs and the pseudo-ETFs for the three sites and each base-case profile, two parameters were estimated. First, the leave-one-out cross-validation error estimator (Q^2) was computed (Blatman and Sudret 2010; Al-Bittar and Soubra 2013). The Q^2 allows the evaluation of the overall fit of TTFs with pseudo-ETFs, a value of 1 indicates a perfect fit over the frequency range of interest. At Mirandola, the average Q^2 over the sets of 200 TTFs is displayed in Table 4 (Tables S3 and S6 in Appendices S2 and S3 for Grenoble and Cadarache, respectively). Larger Q^2 values are systematically obtained for TTFs derived from the Non-Stationary approach indicating a higher fit with pseudo-ETFs, as was already observed visually (Figure 7).

Next, the alignment of the resonance frequency peaks in the TTFs was assessed using Pearson's correlation coefficient (r_p). Ideally, a r_p closer to 1 indicates a perfect correlation between the resonance frequencies, however, a good fit is established when r_p is above 0.6 (Thompson et al. 2012). r_p values were computed between sets of 200 TTFs and corresponding pseudo-ETFs over the frequency range from the first to the fourth resonance frequency peaks. Averaged r_p values over the sets of TTFs are shown in Table 4 for Mirandola and in Appendices S2 and S3 (Tables S3 and S6) for the other two sites. In general, all the TTFs derived from the Non-Stationary approach outline resonance frequencies in agreement with those extracted from pseudo-ETFs, since r_p values were higher than the threshold value of 0.6. Conversely, TTFs derived from Stationary and Toro approaches at Mirandola and Grenoble sites failed to exactly replicate the pseudo-ETFs resonance frequencies since their r_p values were below 0.6 across all profiles.

Overall, the very high agreement between TTFs derived from the Non-Stationary approach and pseudo-ETFs demonstrated the ability of the Non-Stationary approach to generate V_S profiles able to predict the 1D resonance frequencies over a wide frequency range together with their corresponding amplification.

Discussion

The proposed Non-Stationary probabilistic approach allowed the generation of a set of V_S profiles consistent with the pseudo-experimental site signatures in terms of surface-wave dispersion curves, fundamental and higher mode resonance frequencies, and site amplification. This V_S randomization approach outperforms both the classical stationary and the Toro (1995) approaches in terms of compatibility with the dispersion curve including a related predicted variability that is consistent with reported field values (e.g. Comina et al. 2011; Garofalo et al. 2016a; Teague et al. 2018; Passeri et al. 2021), without the need of post-filtering V_S profiles (Toro 1995; Teague et al. 2018). For instance, Teague et al. (2018) obtained a CoV_{Vr} below 5%, when working on experimental dispersion data measured at the Garner Valley downhole array site. They proposed to increase the variability to achieve a CoV_{Vr} of 5% at all frequencies to account for inter-analyst uncertainty. Garofalo et al. (2016a) proposed a range of dispersion CoV_{Vr} between 5 to 10% based on measurements performed at the three InterPACIFIC sites, Mirandola, Grenoble, and Cadarache. Recently, Passeri et al. (2021) reported CoV_{Vr} ranging from 5% at high frequency up to 20% at low frequency from 71 experimental sites in Italy. Since the bedrock depth was fixed in this study, the influence of (1) fixing the layer thicknesses in the Toro (1995) model as the non-stationary approach and (2) varying the bedrock depth as in Toro (1995) was tested to evaluate its impact on the variability of TDCs and TTFs and is presented in Appendix S5. This impact was found to be negligible on the resulting output variability. Moreover, σ_{lnVs} values proposed by Stewart et al. (2014) were employed in the Toro (1995) application here, as done in practice. To investigate the impact of using recommended σ_{lnVs} instead of site-specific σ_{lnVs} on the randomized V_S profiles, a separate set of profiles was generated using the site-specific vertical σ_{lnVs} computed from the soil layers in the base-case V_S profiles. Results of this application, presented in Appendix S5, highlight minor differences in the variability of randomized V_S profiles and their ability to generate sets of consistent site signatures.

The ability of the Non-Stationary method to reproduce site signatures can be explained by its effectiveness in reproducing the shear-wave cumulative travel time. The cumulative travel time represents the time the S-waves take to travel from a certain depth, typically the bedrock interface, to the soil surface. It is directly related to surface-wave dispersion curves and the site response (e.g. Brown et al. 2002; Passeri et al. 2020). The results of this evaluation are presented in Appendix S6 for the Mirandola site. The cumulative travel times exhibited similar behavior as the TDCs and TTFs in terms of the general data trends and scatter around the pseudo-experimental TDCs and TTFs estimates: Non-Stationary travel times converge with low scatter around the borehole travel times, while the Stationary and Toro travel times display systematically higher scatter.

To evaluate the variability of predicted site amplification using the Non-Stationary approach, Figure 8 displays σ_{lnTTF} curves for the three sites. At low frequencies, the variability between sets of TTFs is relatively low compared to that at high frequencies. This behavior at low frequency is expected since randomized V_S profiles reproduce very well both the fundamental resonance frequency and related amplification. Contrarily, velocity heterogeneities induce a scattering effect that results in higher amplitude differences at high frequencies and larger standard deviations in ground motion intensity measures (Thompson et al. 2009; Li and Assimaki 2010; Rathje et al. 2010; Imperatori and Mai 2013; Rodriguez-Marek et al. 2014). Indeed, the scattering by velocity heterogeneities is a frequency-dependent phenomenon that depends on the ratio between the correlation length (θ) of the V_S fluctuations and the seismic wavelength: the scattering is as efficient as the correlation length is larger than the wavelength. In our study, since the correlation length is fixed to 2 m, scattering will occur at high frequencies. In Mirandola and Grenoble, significant scattering will occur for frequencies larger than 4 to 5 Hz while, for Cadarache, only frequencies larger than 20 Hz will exhibit scattering as a result of larger V_S. Although θ was fixed in this study for the sake of simplicity and to focus on the impact of the variable CoV_{Vs} only, varying θ following the quantified values in each layer of the soil profiles

produces minor differences in the high-frequency range corresponding to θ larger than the seismic wavelength.

Note also that differences in the quantification of V_S variability in terms of CoV_{Vs} between distinct base-case profiles and various layers (Table 2 for Mirandola and Tables S2 and S5 in Appendices S2 and S3 for Grenoble and Cadarache, respectively) propagate to differences in the variability of site response estimates (Figure 8). While higher σ_{lnTTF} were found to be relative to PS-SL tests in Mirandola, higher σ_{lnTTF} in Grenoble correspond to DH tests (Figure 8 (a) and (b)). The base-case profile dependency of σ_{lnTTF} indicates that the V_S measurement method and the quantification of V_S variability inside each soil layer have a significant influence on the propagation of V_S uncertainty into the variability of site response.

Conclusion

In the present work, a novel shear-wave velocity (V_S) randomization approach is proposed to propagate aleatory V_S variability into samples of V_S profiles within a non-stationary probabilistic framework. The primary interest of the method is to account for the natural spatial variability of soil properties in a rigorous manner. The formulation of the non-stationary approach is founded on partitioning a base-case V_S profile acquired from invasive testing into several locally stationary layers allowing the transformation of the non-stationary random field (RF) into multiple small-scale stationary RFs. Then, the vertical variability of V_S is quantified for each layer and its statistical parameters (i.e., coefficient of variation, scale of fluctuation) can be used to discretize the RF of V_S. The discretization of the RF is realized using the Expansion Optimal Linear Estimation method and multiple realizations are then generated to obtain a set of randomized V_S profiles.

The proposed approach was applied to three European sites for which V_S profiles from various invasive measurements (PS-SL, CH, DH) are available, and compared to other common approaches used for randomizing V_S, namely the classical stationary probabilistic approach and the Toro (1995) approach. The non-stationary V_S randomization approach was found to accurately replicate site

signatures in terms of dispersion curves, resonance frequencies, and site amplification over a wide frequency range. In this matter, the proposed method resulted in V_S profiles and corresponding site signatures closely distributed around experimental borehole data, including S-wave cumulative travel time. The variability in the results is lower than that obtained from the other two approaches, which strongly implies that there is no need to perform any posterior selection of V_S to avoid accounting for unrealistic V_S profiles (Toro 1995; Teague et al. 2018). Note that in this paper the V_S profiles were generated using a base-case V_S profile, and borehole logs were used to partition the V_S layers. However, the approach is more generic since the V_S statistics (μ_{Vs}, CoV_{Vs}) can be estimated by some other method, e.g. from the vertical evolution of V_S profiles available from invasive or surface-wave methods. This choice is not expected to affect the performance of the RF discretization method itself but the resulting variability in V_S profiles that will be controlled by the imposed CoV_{Vs}.

The findings of this study highlighted that attention should be paid to the choice of V_S measurement method since it has an impact on both the measured variability of V_S and the predicted site response variability. In this study, the largest coefficient of variation for V_S was overall found in PS-SL profiles since this measurement method provides a higher vertical resolution compared to DH and CH measurements. Besides, within a given geological layer, the quantification of V_S variability was found to be strongly influenced by the measurement method, with differences between methods of up to 90-130%. Such V_S variability translated into variability of predicted site amplification, with higher amplification variability at high frequency as a consequence of both scattering effects by velocity heterogeneities and the level of V_S variability.

Although the non-stationary V_S randomization approach yields a promising straightforward method to account for the aleatory spatial variability of V_S in 1D ground response analysis, the approach must be further validated at well instrumented downhole array sites. Indeed, the use of recorded weak ground motions at the surface and in depth at a site prone to 1D seismic wave propagation will allow evaluation of the compatibility of predicted site response with the empirical site amplification and related variabilities. Such evaluation is essential to further assess any potential under or overestimation of site

response variability and its implications on the V_S randomization performance. This will also help in better understanding the effects of V_S variability in each layer on the surface ground motion variability. Furthermore, future developments of the proposed approach should move beyond 1D applications to embrace complex wave propagation effects (body and surface waves diffraction, wave scattering, and mode conversion, etc.) and 2D/3D V_S heterogeneities.

Data Availability Statement

The codes developed for the spatial variability quantification of the shear-wave velocity and the random field discretization are available online in a GitLab repository with detailed commentary, hosted at `https://gricad-gitlab.univ-grenoble-alpes.fr/youssefe/variability-quantification-and-discretization-of-random-fields`. The sets of shear-wave velocity profiles developed at the InterPACIFIC sites are also available from the corresponding author upon request.

Acknowledgments

This work benefited from the support and funding provided by the IRD (France) through the ARTS program, the Lebanese University and the University of Grenoble Alpes. The authors are also thankful for three anonymous reviewers, Editorial Board Member Robb Eric Moss, and Associate Editor, for their invaluable feedback, which greatly contributed to improving the quality and clarity of this manuscript.

References

Al-Bittar, T., and A.-H. Soubra. 2013. "Bearing capacity of strip footings on spatially random soils using sparse polynomial chaos expansion." *Int. J. Numer. Anal. Meth. Geomech.* 37 (13), 2039-2060. https://doi.org/10.1002/nag.2120

Al-Bittar, T., A.-H. Soubra, and J. Thajeel. (2018). "Kriging-based reliability analysis of strip footings resting on spatially varying soils." *J. Geotech. Geoenviron. Eng.* 144(10): 04018071. doi:10.1061/(ASCE)GT.1943-5606.0001958

Assimaki, D., Pecker, A., Popescu, R., and Prevost, J. 2003. "Effects of spatial variability of soil properties on surface ground motion." *J. Earthq. Eng*. 7(1), 1–44. https://doi.org/10.1142/S1363246903000973

Baise, L., E. M. Thompson, J. Kaklamanos, and L. Dorfmann. 2011. "Complex site response: Does one-dimensional site response work." In Proc., 4th Int. Sym. on the Effects of Surface Geology on Seismic Motion. International Association of Seismology and Physics of the Earth's Interior and International

Association of Earthquake Engineering, University of California, Santa Barbara.Blatman, G., and B. Sudret. 2010. “An adaptive algorithm to build up sparse polynomial chaos expansions for stochastic finite element analysis.” *Probabilistic Eng. Mech*. 25 (2), 183-197.

Brown, L. T., D. M. Boore, and K. H. Stokoe. 2002. “Comparison of shear-wave slowness profiles at 10 strong-motion sites from noninvasive SASW measurements and measurements made in boreholes.” *Bull. Seismol. Soc. Am*. 92, 3116-3133.

Comina, C., S. Foti, D. Boiero, and L. V. Socco. 2011. “Reliability of VS30 evaluation from surface-wave tests”. *J. Geotech. Geoenviron. Eng*. 137(6), 579-586.

DeGroot, D. J. 1996. “Analyzing spatial variability of in situ soil properties”. In Uncertainty in the geologic environment: From theory to practice, 210-238. ASCE.

De la Torre, C., B. Bradley, and C. McGann. 2022. “2D Geotechnical site-response analysis including soil heterogeneity and wave scattering.” *Earthquake Spectra*. 38(2), 1124-1147. doi:10.1177/87552930211056667

De Martin, F., E. Chaljub, P. Thierry, P. Sochala, F. Dupros, E. Maufroy, B. Hadri, A. Benaichouche, F. Hollender. 2021. “Influential parameters on 3-D synthetic ground motions in a sedimentary basin derived from global sensitivity analysis.” Geophys. J. Int. 227 (3): 1795–1817. https://doi.org/10.1093/gji/ggab304

Einsele, G. 2000. Sedimentary basins: evolution, facies, and sediment budget. New York: Springer.

El Haber, E., C. Cornou, D. Jongmans, D. Y. Abdelmassih, F. Lopez-Caballero, and T. Al-Bittar. 2019. “Influence of 2D heterogeneous elastic soil properties on surface ground motion spatial variability”. *Soil Dyn. Earthquake Eng*. 123, 75-90.

Fenton, G. 1999. “Random field modeling of CPT data.” J. Geotech. Geoenviron. Eng. 125 (6): 486-498. https://doi.org/10.1061/(ASCE)1090-0241(1999)125:6(486).

Foti, S., F. Hollender, F. Garofalo, D. Albarello, M. Asten, P. Y. Bard, C. Comina, C. Cornou, B. Cox, G. Di Giulio, T. Forbriger, K. Hayashi, E. Lunedei, A. Martin, D. Mercerat, M. Ohrnberger, V. Poggi, F. Renalier, D. Sicilia & V. Socco. (2018). “Guidelines for the good practice of surface wave analysis: a product of the InterPACIFIC project.” *Bull. Earthq. Eng*. 16, 2367-2420.

Garofalo, F., S. Foti, F. Hollender, P. Y. Bard, C. Cornou, B. R. Cox, M. Ohrnberger, D. Sicilia, M. Asten, G. Di Giulio, T. Forbriger, B. Guillier, K. Hayashi, A. Martin, S. Matsushima, D. Mercerat, V. Poggi, H. Yamanaka. 2016a. “InterPACIFIC project: Comparison of invasive and non-invasive methods for seismic site characterization. Part I: Intra-comparison of surface wave methods.” *Soil Dyn. Earthquake Eng*. 82, 222-240.

Garofalo, F., S. Foti, F. Hollender, P. Y. Bard, C. Cornou, B. R. Cox, A. Dechamp, M. Ohrnberger, D. Sicilia and C. Vergniault. 2016b. “InterPACIFIC project: Comparison of invasive and non-invasive methods for seismic site characterization. Part II: Inter-comparison between surface-wave and borehole methods.” *Soil Dyn. Earthquake Eng*. 82, 241-254.

Griffiths, D., J. Huang, and G. Fenton. (2009). "Influence of Spatial Variability on Slope Reliability Using 2-D Random Fields." *J. Geotech. Geoenviron. Eng*. 135(10). doi:10.1061/(ASCE)GT.1943-5606.0000099

Griffiths, S. C., B. R. Cox, E. M. Rathje, and D. P. Teague. 2016a. “Surface-wave dispersion approach for evaluating statistical models that account for shear-wave velocity uncertainty.” *J. Geotech. Geoenviron. Eng.* 142(11): 04016061. https://doi.org/10.1061/(ASCE)GT.1943-5606 .0001552.

Griffiths, S. C., B. R. Cox, E. M. Rathje, and D. P. Teague. 2016b. “Mapping dispersion misfit and uncertainty in Vs profiles to variability in site response estimates.” *J. Geotech. Geoenviron. Eng.* 142(11): 04016062. https://doi.org/10.1061/(ASCE)GT.1943-5606.0001553.

Haldar, S., and G. S. Babu. 2008. “Effect of soil spatial variability on the response of laterally loaded pile in undrained clay.” *Computers and Geotechnics*. 35 (4), 537-547.

Hallal, M. M., and B. R. Cox. 2021. “An H/V Geostatistical Approach for Building Pseudo-3D Vs Models to Account for Spatial Variability in Ground Response Analyses II: Application to 1D analyses at two downhole array sites.” *Earthquake Spectra*. 37 (3): 1931–1954. https://doi.org/10.1177/8755293020981982.

Hallal, M. M., B. R. Cox, S. Foti, A. Rodriguez-Marek, and E. R. Rathje. 2022a. "Improved implementation of the travel time randomization method for incorporating Vs uncertainty in ground response analyses." *Soil Dyn. Earthquake Eng*. 157:107277. https://doi.org/10.1016/j.soildyn.2022.107277

Hallal, M. M., B. R. Cox, and J. Vantasel. 2022b. “Comparison of State-of-the-Art Approaches Used to Account for Spatial Variability in 1D Ground Response Analyses”. *J. Geotech. Geoenviron. Eng*. 148(5): 04022019. https://doi.org/10.1061/(ASCE)GT.1943-5606.0002774.

Hallo, M., P. Bergamo, and D. Fäh. 2022. “Stochastic Model to Characterize High-Frequency Ground Motion at Depth Validated by KiK-Net Vertical Array Data.” *Bull. Seismol. Soc. Am.* 112, 1997–2017, doi: 10.1785/0120220038

Imperatori, W., and P. M. Mai. 2013. “Broad-band near-field ground motion simulations in 3-dimensional scattering media.” *Geophys. J. Int*. 192, 725–744.

Jaksa, M. B. 1995. “The influence of spatial variability on the geotechnical design properties of a stiff, overconsolidated clay.” Ph.D. thesis, Univ. of Adelaide, Dept. of Civil and Environmental Engineering, Adelaide, Australia.

Jamshidi Chenari, R., and H. Kamyab Farahbakhsh. 2015. “Generating non-stationary random fields of auto-correlated, normally distributed CPT profile by matrix decomposition method.” Georisk: Assessment and Management of Risk for Engineered Systems and Geohazards 9 (2): 96–108. https://doi.org/10.1080/17499518.2015.1033429

Jamshidi Chenari, R., H. Kamyab Farahbakhsh, S. Heidarie Golafzani, and Eslami, A. 2018. “Non-stationary realisation of CPT data: considering lithological and inherent heterogeneity.” Georisk: Assessment and Management of Risk for Engineered Systems and Geohazards 12 (4): 265–278. https://doi.org/10.1080/17499518.2018.1447675

Jiang, S., and J. Huang. 2018. “Modeling of non-stationary random field of undrained shear strength of soil for slope reliability analysis.” *Soils and Foundations*. 58(1), 185-198.

Kaklamanos, J., and B. A. Bradley. 2018. “Challenges in Predicting Seismic Site Response with 1D Analyses: Conclusions from 114 KiK-net Vertical Seismometer Arrays.” *Bull. Seismol. Soc. Am*. 108(5), 2816-2838. https://doi.org/10.1785/0120180062

Kaklamanos, J., B. A. Bradley, A. N. Moolacattu, and B. M. Picard. 2020. “Physical hypotheses for adjusting coarse profiles and improving 1D site-response estimation assessed at 10 KiK-net sites.” *Bull. Seismol. Soc. Am*. 110 (3): 1338–1358. https://doi.org/10.1785/0120190263

Kennet, B. 1983. *Seismic wave propagation in stratified media*. Canberra, Australia: ANU Press.

Kleiber, W. 2016. “High resolution simulation of nonstationary Gaussian random fields.” *Comput. Stat. Data Anal.* 101, 277-288. https://doi.org/10.1016/j.csda.2016.03.005.

Kottke, A., and E. Rathje. 2009. *Technical manual for Strata*. PEER Report 2008/10. Berkley, California: Pacific Earthquake Engineering Research Center.

Kramer, S. L. 1996. *Geotechnical Earthquake Engineering*. Upper Saddle River, NJ: Prentice Hall.

Laurendeau, A., P. Y. Bard, F. Hollender, V. Perron, L. Foundotos, O. J. Ktenidou, & B. Hernandez. 2018. “Derivation of consistent hard rock (1000< VS< 3000 m/s) GMPEs from surface and down-hole recordings: analysis of KiK-net data.” *Bull. Earthq. Eng*. 16, 2253-2284.

Li, C. -C., and A. Der Kiureghian. 1993. “Optimal discretization of random fields.” *J. of Eng. Mechanics*. 119(6), 1136-1154. https://doi.org/10.1061/(ASCE)0733-9399(1993)119:6(1136).

Li, W., and D. Assimaki. 2010. “Site-and motion-dependent parametric uncertainty of site-response analyses in earthquake simulations.” *Bull. Seismol. Soc. Am*. 100(3), 954-968.

Montoya-Noguera, S., T. Zhao, Y. Hu, Y. Wang, K. -K. Phoon. 2019. “Simulation of non-stationary non-Gaussian random fields from sparse measurements using Bayesian compressive sampling and Karhunen-Loève expansion.” *Structural Safety*. 79, 66-79.

Nour, A., A. Slimani, N. Laouami, and H. Afra. 2003. “Finite element model for the probabilistic seismic response of heterogeneous soil profile.” *Soil Dyn. Earthquake Eng.* 23, 331-348.

Pagliaroli, A., M. Moscatelli, G. Raspa, and G. Naso. 2014. “Seismic microzonation of the central archaeological area of Rome: results and uncertainties.” *Bull. Earthq. Eng.* 12, 1405-1428.

Parolai, S., D. Bindi, and M. Pilz. 2015. “k0: the role of intrinsic and scattering attenuation.” *Bull. Seismol. Soc. Am*. 105, 1049–1052.

Passeri, F., C. Comina, L.V. Socco, and S. Foti. 2021. “The Polito Surface Wave flat-file Database (PSWD): statistical properties of test results and some inter-method comparisons.” *Bull. Earthquake. Eng*. 19, 2343–2370. https://doi.org/10.1007/s10518-021-01069-1

Passeri, F., S. Foti, and A. Rodriguez-Marek. 2020. “A new geostatistical model for shear wave velocity profiles.” *Soil Dyn. Earthquake Eng*. 136: 106247. https://doi.org/10.1016/j.soildyn.2020.106247.

Peng, B., J. Xu, and Y. Peng. 2022. “Efficient simulation of multivariate non-stationary ground motions based on a virtual continuous process and EOLE.” *Mech. Syst. Signal Process*. *184*. https://doi.org/10.1016/j.ymssp.2022.109722

Phoon, K.-K., and F. H. Kulhawy. 1996. “On quantifying inherent soil variability.” Geotechnical Special Publication (58 I): 326-340. http://scholarbank.nus.edu.sg/handle/10635/65923

Phoon, K.-K., and F. H. Kulhawy. 1999a. “Characterization of Geotechnical Variability.” *Can. Geotech. J.* 36(4), 612-624. https://doi.org/10.1139/t99-038.

Phoon, K.-K., and F. H. Kulhawy. 1999b. “Evaluation of Geotechnical Property Variability.” *Can. Geotech. J.* 36(4), 625-639. https://doi.org/10.1139/t99-039.

Pilz, M., and D. Fäh. 2017. “The contribution of scattering to near-surface attenuation.” *J. Seismol*. 21, 837–855. https://doi.org/10.1007/s10950-017-9638-4

Pilz, M., and F. Cotton. 2019. “Does the one-dimensional assumption hold for site response analysis? A study of seismic site responses and implication for ground motion assessment using KiK-net strong-motion data.” *Earthquake Spectra.* 35 (2), 883–905. https://doi.org/10.1193/050718EQS113M.

Popescu, R. 1995. “Stochastic variability of soil properties: Data analysis, digital simulation, effects on system behavior.” Ph.D. thesis, Princeton Univ., Dept. of Civil and Environmental Engineering, New Jersey, USA.

Rathje, E. M., A. R. Kottke, and W. L. Trent. 2010. “Influence of input motion and site property variabilities on seismic site response analysis.” *J. Geotech. Geoenviron. Eng.* 136(4), 607-19. https://doi.org/10.1061/(ASCE)GT.1943-5606.0000255.

Rodriguez-Marek, A., E. M. Rathje, J. J. Bommer, F. Scherbaum, and P. J. Stafford. "Application of single-station sigma and site-response characterization in a probabilistic seismic-hazard analysis for a new nuclear site." Bull. Seismol. Soc. Am. 104 (4): 1601-1619. http://hdl.handle.net/2152/43265

Salloum, N. 2015. “Evaluation de la variabilité spatiale des paramètres géotechniques du sol à partir de mesures géophysiques : application à la plaine alluviale de Nahr-Beyrouth (Liban).” Ph.D. thesis, Univ. Joseph Fourier, ISTerre, Grenoble, France.

Shi, J., and D. Assimaki. (2018). “A generic velocity profile for basin sediments in California conditioned on VS30.” *Seismol. Res. Lett*. 89, 1397-1409.

Socco, L. V., and C. Strobbia. (2004). “Surface-wave method for near-surface characterization: A tutorial.” Near surface geophysics. 2(4), 165-185.

Soubra, A.-H. and D. Youssef Abdel Massih. 2009. “Probabilistic analysis and design at the ultimate limit state of obliquely loaded strip footings.” *Géotechnique*. *ICE*. 60(4), 275–285.

Stewart J., K. Afshari, and Y. Hashash. 2014. *Guidelines for performing hazard-consistent one-dimensional ground response analysis for ground motion prediction*. Berkely, California: Pacific Earthquake Engineering Research Center.

Sudret, B., and A. Der Kiureghian. 2000. *Stochastic finite element methods and reliability: a state-of-the-art report*. Berkley, California: Department of Civil and Environmental Engineering, University of California.

Tao, Y., and E. Rathje. 2019. “Insights into Modeling Small-Strain Site Response Derived from Downhole Array Data.” *J. Geotech. Geoenviron. Eng.* 145(7). https://doi.org/10.1061/(ASCE)GT.1943-5606.0002048.

Tao, Y., and E. Rathje. 2020. “Taxonomy for evaluating the site-specific applicability of one-dimensional ground response analysis.” *Soil Dyn. Earthquake Eng*. 128: 288-294. https://doi.org/10.1016/j.soildyn.2019.105865.

Tchawe, F. N., C. Gelis, L. F. Bonilla, and F. Lopez-Caballero. 2021. “Effects of 2-D random velocity perturbations on 2-D SH short-period ground motion simulations in the basin of Nice, France.” *Geophys. J. Int*. 226(2), 847-861. https://doi.org/10.1093/gji/ggab141.

Teague, D. P., and B. R. Cox. 2016. “Site response implications associated with using non-unique Vs profiles from surface wave inversion in comparison with commonly used methods of accounting for Vs uncertainty.” *Soil Dyn. Earthquake Eng*. 91, 87-103.

Teague, D. P., B. R. Cox, and E. M. Rathje. 2018. “Measured vs. predicted site response at the Garner Valley Downhole Array considering shear wave velocity uncertainty from borehole and surface wave methods.” *Soil Dyn. Earthquake Eng*. 113, 339–355.

Thompson, E. M., L. G. Baise, R. E. Kayen, and B. B. Guzina. 2009. “Impediments to predicting site response: Seismic property estimation and modeling simplifications.” *Bull. Seismol. Soc. Am.* 99 (5), 2927–2949. https://doi.org/10.1785/0120080224.

Thompson, E., L. Baise, Y. Tanaka, R. Kayen. 2012. “A taxonomy of site response complexity.” *Soil Dyn. Earthquake Eng*. 41, 32-43. https://doi.org/10.1016/j.soildyn.2012.04.005.

Toro, G. 1995. *Probabilistic models of the site velocity profiles for generic and site-specific ground-motion amplification studies*. Technical Rep. 779574. New York: Brookhaven National Laboratory.

Toro, G. 2022. “Uncertainty in Shear-Wave Velocity Profiles.” J. Seismol. 26, 713–730.

Vanmarcke, E. 1983. *Random fields: analysis & synthesis*. Cambridge: The MIT Press.

Vantassel, J. P., and B. R. Cox. 2021. “A procedure for developing uncertainty-consistent vs profiles from inversion of surface wave dispersion data.” *Soil Dyn. Earthquake Eng.* 145: 106622.

Wathelet, M., D. Jongmans, and M. Ohrnberger. 2004. “Surface-wave inversion using a direct search algorithm and its application to ambient vibration measurements.” *Near surface geophysics*. 2, 211-221.

Wathelet, M., J.-L. Chatelain, C. Cornou, G. Di Giulio, B. Guillier, M. Ohrnberger, A. Savvaidis. (2020). "Geopsy: A User-Friendly Open-Source Tool Set for Ambient Vibration Processing." *Seismol. Res. Lett*. 91, 1878-1889.

Youssef Abdel Massih, D. 2007. “Analyse du comportement des fondations superficielles filantes par des approches fiabilistes.” Ph.D. thesis, Univ. of Nantes, Faculté des sciences et des techniques, Nantes, France.

Zalachoris, G., and E. Rathje. 2015. "Evaluation of One-Dimensional Site Response Techniques Using Borehole Arrays." *J. Geotech. Geoenviron. Eng*. 141(12), 04015053. https://doi.org/10.1061/(ASCE)GT.1943-5606.0001366.

Tables

Table 1. Vertical scale of fluctuation θ (m) for each layer (layer numbering ordered from surface to depth) in the six base-case borehole V_S profiles in Mirandola site. Also shown are the average (μ) and CoV of θ for each layer.

Layer	Thickness (m)	Parameter	PS-SL S-R1	PS-SL R1-R2	DH-EW	DH-NS	CH1	CH2	$\mu_{(\theta)}$	$CoV_{(\theta)}$
1	4	θ_1	0.27	0.86	0.83	0.83	0.86	1.34	0.83	40.96
2	6	θ_2	1.33	1.31	1.69	1.69	1.78	0.61	1.40	31.43
3	15	θ_3	1.46	1.29	4.37	4.46	1.40	2.15	2.52	59.52
4	25.5	θ_4	4.93	0.64	2.97	2.30	1.84	3.41	2.68	54.48
5	9	θ_5	1.09	0.94	2.66	2.66	2.21	0.92	1.75	48.57
6	6	θ_6	1.20	0.68	1.16	0.52	1.12	1.55	1.04	36.54
7	3.5	θ_7	0.62	0.67	0.76	0.75	0.78	0.96	0.76	15.79
8	6	θ_8	1.46	1.41	1.38	1.03	1.35	1.87	1.42	19.01
9	21	θ_9	2.23	2.33	5.48	5.48	2.62	2.97	3.52	43.75
10	16	θ_{10}	1.10	0.52	4.77	4.69	3.10	3.36	2.92	60.96

Table 2. Coefficient of variation CoV_{Vs} (%) for each layer (layer numbering ordered from surface to depth) in the six base-case borehole V_S profiles in Mirandola site with the number of V_S samples indicated in parentheses for each layer. Also shown are the average (μ) and CoV of CoV_{Vs} for each layer.

Layer	Parameter	PS-SL S-R1	PS-SL R1-R2	DH-EW	DH-NS	CH1	CH2	$\mu_{(CoV)}$	$CoV_{(CoV)}$
1	CoV_1	4.81(3)	12.10(6)	0.01(9)	0.01(9)	3.31(4)	1.28(4)	3.59	127.58
2	CoV_2	12.09(11)	22.31(11)	15.85(11)	11.63(11)	16.76(7)	4.84(7)	13.91	42.27
3	CoV_3	9.30(31)	14.50(31)	4.76(31)	7.55(31)	5.90(16)	6.41(16)	8.07	43.49
4	CoV_4	10.51(51)	10.96(51)	6.77(51)	6.34(51)	8.36(27)	9.00(27)	8.66	21.82
5	CoV_5	16.32(18)	19.37(18)	13.09(18)	14.06(18)	13.65(9)	12.21(9)	14.78	17.79
6	CoV_6	7.53(11)	10.29(11)	7.94(11)	7.94(11)	3.91(7)	4.24(7)	6.98	35.10
7	CoV_7	3.71(9)	9.11(9)	0.01(9)	0.01(9)	4.19(5)	2.48(5)	3.25	104.00
8	CoV_8	37.70(10)	38.70(10)	28.15(10)	19.16(10)	10.39(6)	9.15(6)	23.88	54.61
9	CoV_9	12.07(43)	19.89(43)	2.68(43)	9.97(43)	10.72(22)	5.82(22)	10.19	57.80
10	CoV_{10}	5.32(32)	9.01(32)	0.56(32)	7.46(32)	11.62(17)	8.04(17)	7.00	53.86

Table 3. Velocity, layering, and depth to bedrock model parameters for the Toro (1995) V_S randomization approach applied for the six base-case V_S profiles in each of Mirandola, Grenoble and Cadarache sites.

Model	*Parameter*	*Mirandola*	*Grenoble*	*Cadarache*
Velocity	V_{S30}[a] (m/s)	195 - 216	331 - 373	1562 - 1963
	Soil class	C	B C	A
	σ_{lnVs} ($z \leq 50$ m)	0.15	0.15	0.15
	σ_{lnVs} ($z > 50$ m)	0.22	-	-
	ρ_0[b]	0.99	0.97 0.99	0.95
	ρ_{200}[c]	0.98	1 0.98	0.42
	Δ[b]	3.9	3.8 3.9	3.4
	h_0[c]	0	0	0
	b[c]	0.34	0.29 0.34	0.06
Layering	Density (kg/m^3)	1800	1800	2200
	c_1[d]	10.86	10.86	10.86
	c_2[d]	0.89	0.89	0.89
	c_3[d]	1.98	1.98	1.98
Depth to bedrock	Distribution	Fixed	Fixed	Fixed
	Z bedrock (m)	112	45	31
	V_S bedrock (m/s)	1000	1000	3200
	V_P bedrock (m/s)	3000	2000	5536
	Density (kg/m^3)	2500	2500	2500

a: V_{S30} = Time-averaged shear-wave velocity in the topmost 30 m.
b: ρ_0 and Δ are model parameters used for the calculation of the thickness-dependent correlation.
c: ρ_{200}, h_0 and b are model parameters used for the calculation of the depth-dependent correlation.
d: c_1, c_2 and c_3 are model parameters of the modified power law for the non-homogeneous Poisson process for the layer randomizations ($\lambda(z) = c_3(z + c_1)^{-c_2}$, z is the depth in m).

Table 4. Average determination coefficient Q^2 for the leave-one-out cross-validation error and average Pearson's sample correlation coefficient r_p over the 200-sets of non-stationary, stationary and the Toro (1995) theoretical transfer functions (TTFs) for six base-case profiles compared to corresponding pseudo-experimental transfer functions for Mirandola site.

V_S profile	Q^2			r_p		
Mirandola	Non-stationary	Stationary	Toro (1995)	Non-stationary	Stationary	Toro (1995)
PS-SL S-R1	0.872	0.679	0.838	0.948	0.437	0.412
PS-SL R1-R2	0.817	0.655	0.864	0.880	0.304	0.349
DH-EW	0.910	0.709	0.890	0.969	0.263	0.370
DH-NS	0.932	0.716	0.886	0.977	0.299	0.368
CH1	0.934	0.769	0.902	0.972	0.593	0.414
CH2	0.951	0.730	0.913	0.969	0.504	0.393

Figures

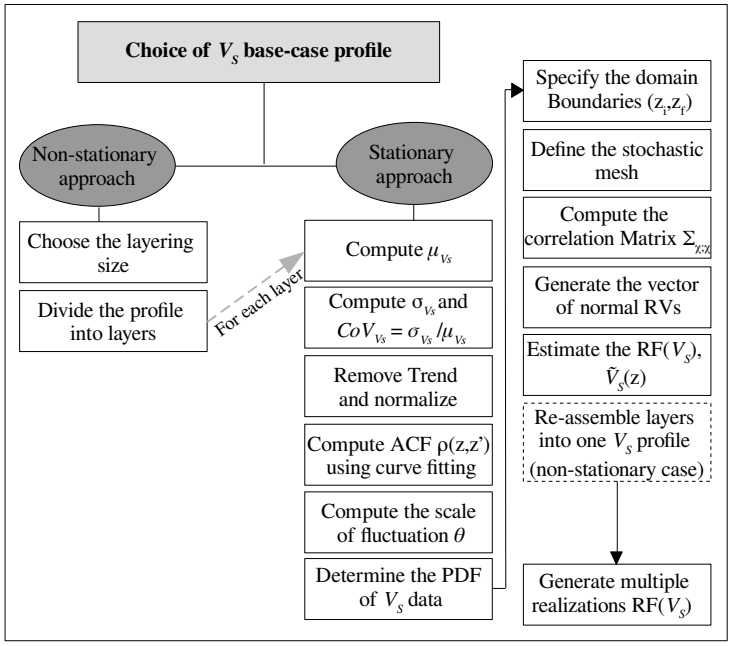

Fig. 1. Procedure for generating stationary and non-stationary realizations of V_S random fields.

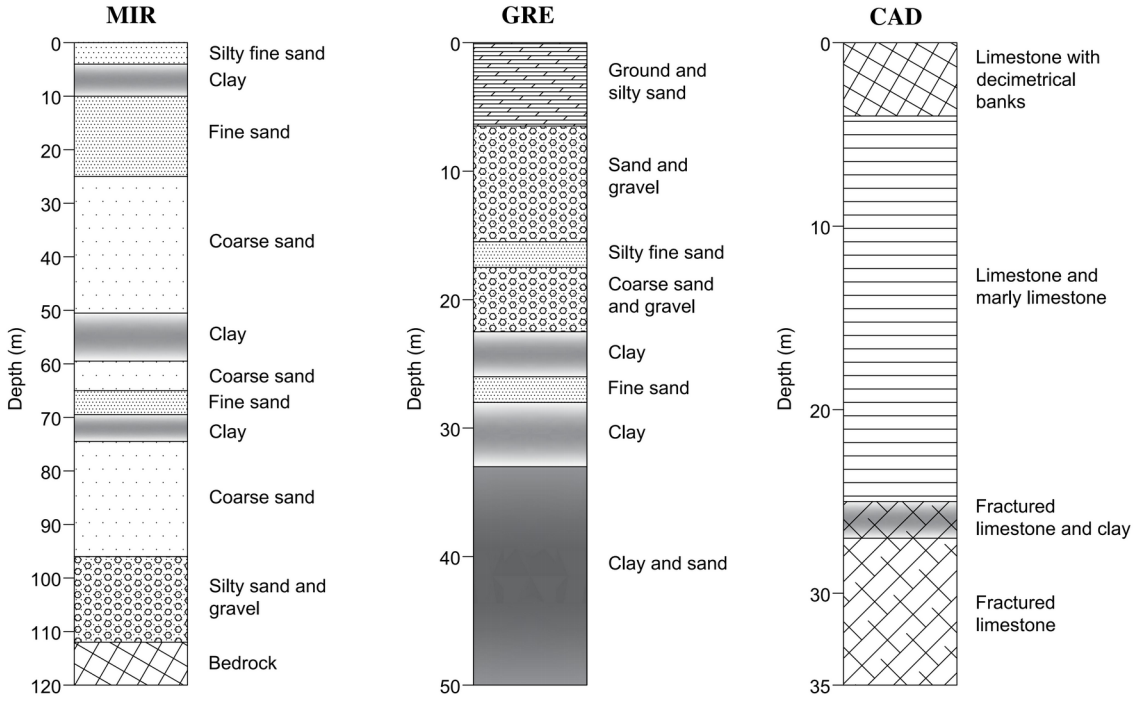

Fig. 2. Soil stratigraphy at (a) Mirandola, Italy; (b) Grenoble, France; and (c) Cadarache, France, sites, from left to right. Depth scales are site dependent. (Data from Garofalo et al. 2016b).

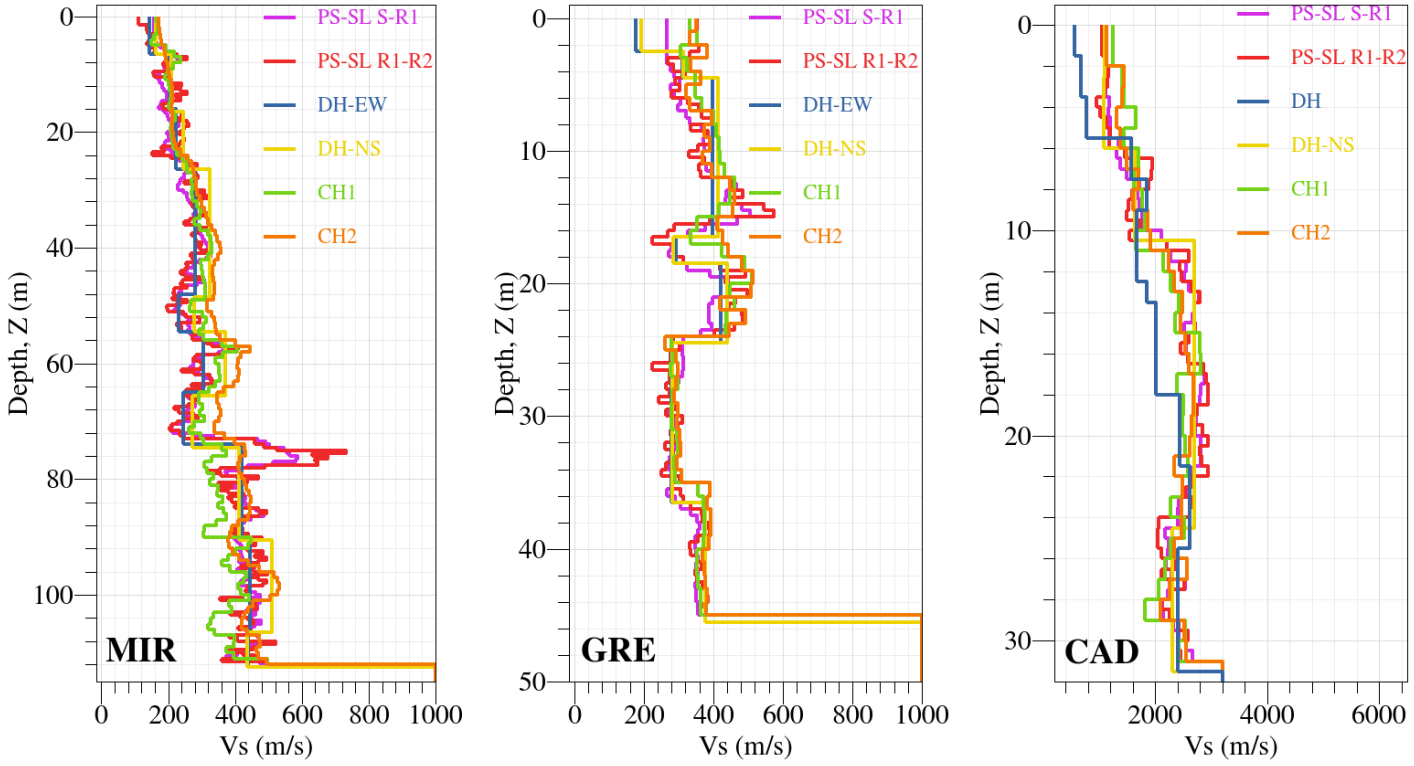

Fig. 3. Borehole base-case V_S profiles at Mirandola (MIR); Grenoble (GRE); and Cadarache (CAD) sites, from left to right.

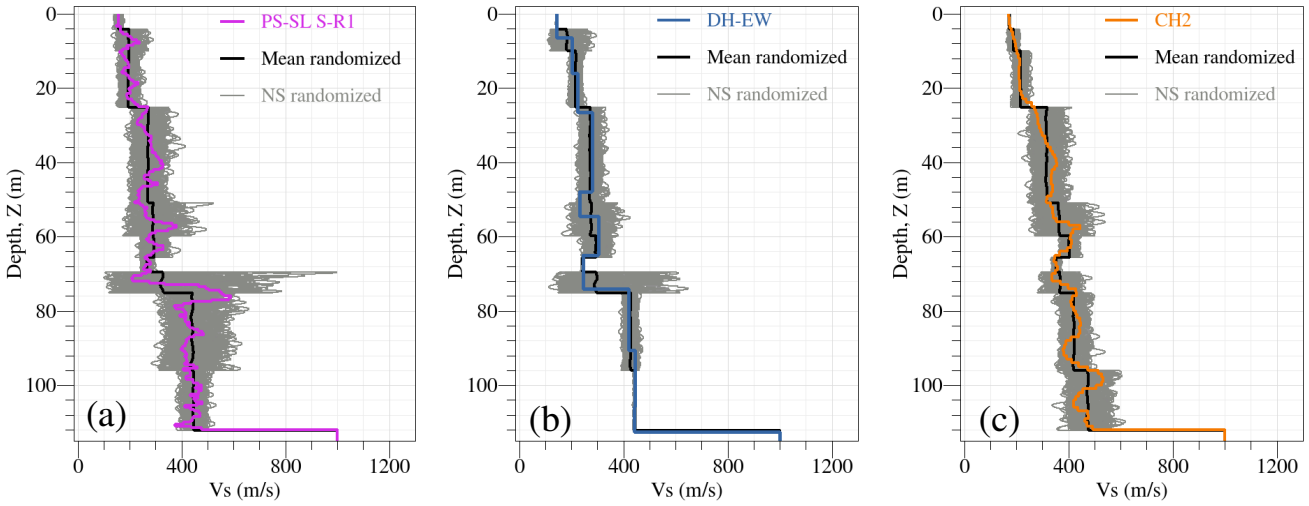

Fig. 4. Generated suites of 200 V_S profiles (grey curves) following the proposed non-stationary approach for three base-case V_S profiles at Mirandola: (a) PS-SL S-R1; (b) DH-EW; and (c) CH2 alongside the average randomized profile (solid black curve). The invasively-measured base-case V_S profiles at Mirandola are indicated in color.

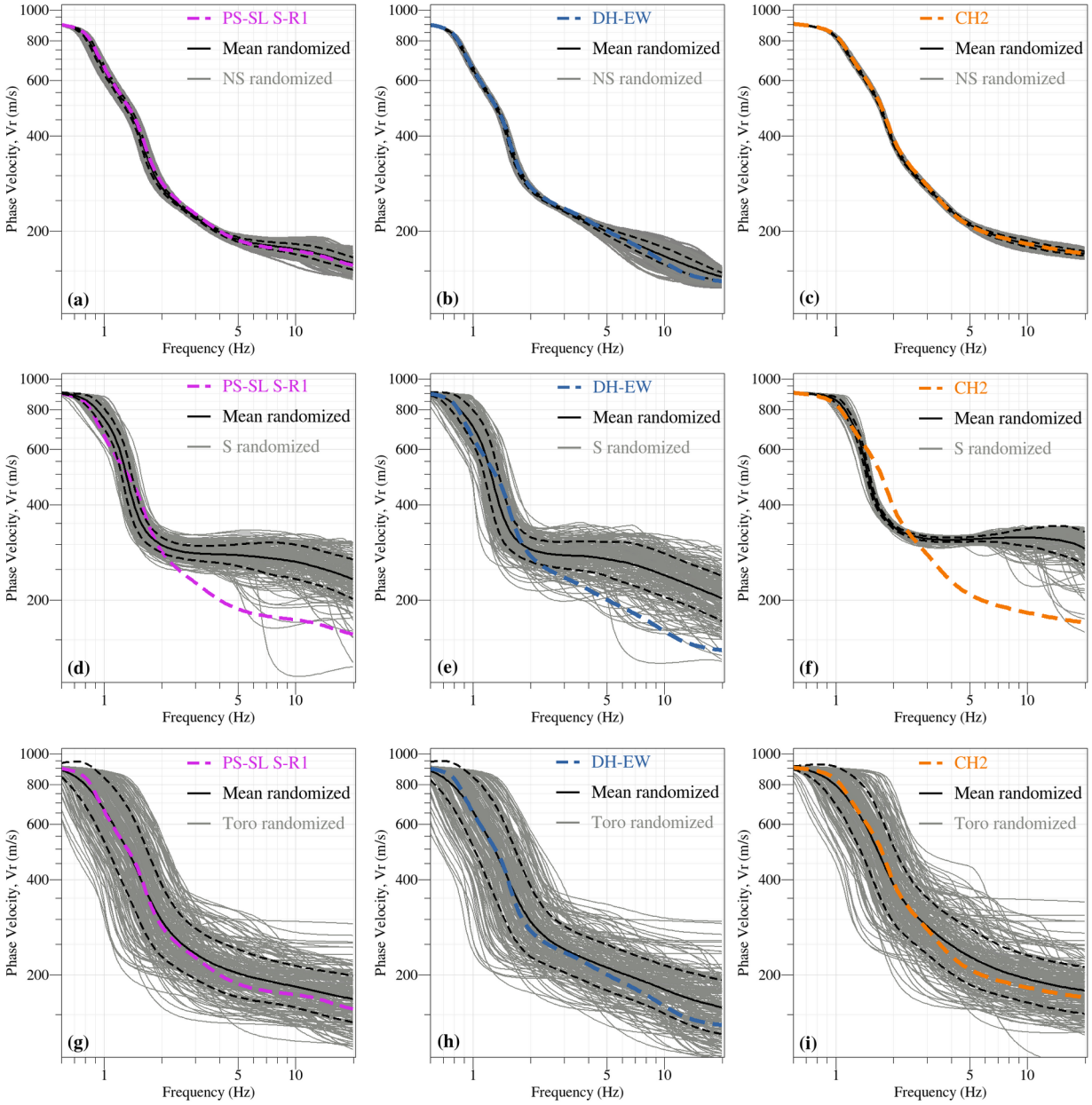

Fig. 5. The 200-sets of theoretical dispersion curves calculated from (a-c) non-stationary; (d-f) stationary; and (g-i) Toro (1995) randomized profiles for three base-case V_S profiles alongside their mean randomized TDCs (solid black line) and related standard deviations ± 1σ (dotted black lines). Also shown in dotted colored curves the pseudo-experimental DCs computed from the three base-case V_S profiles at Mirandola site.

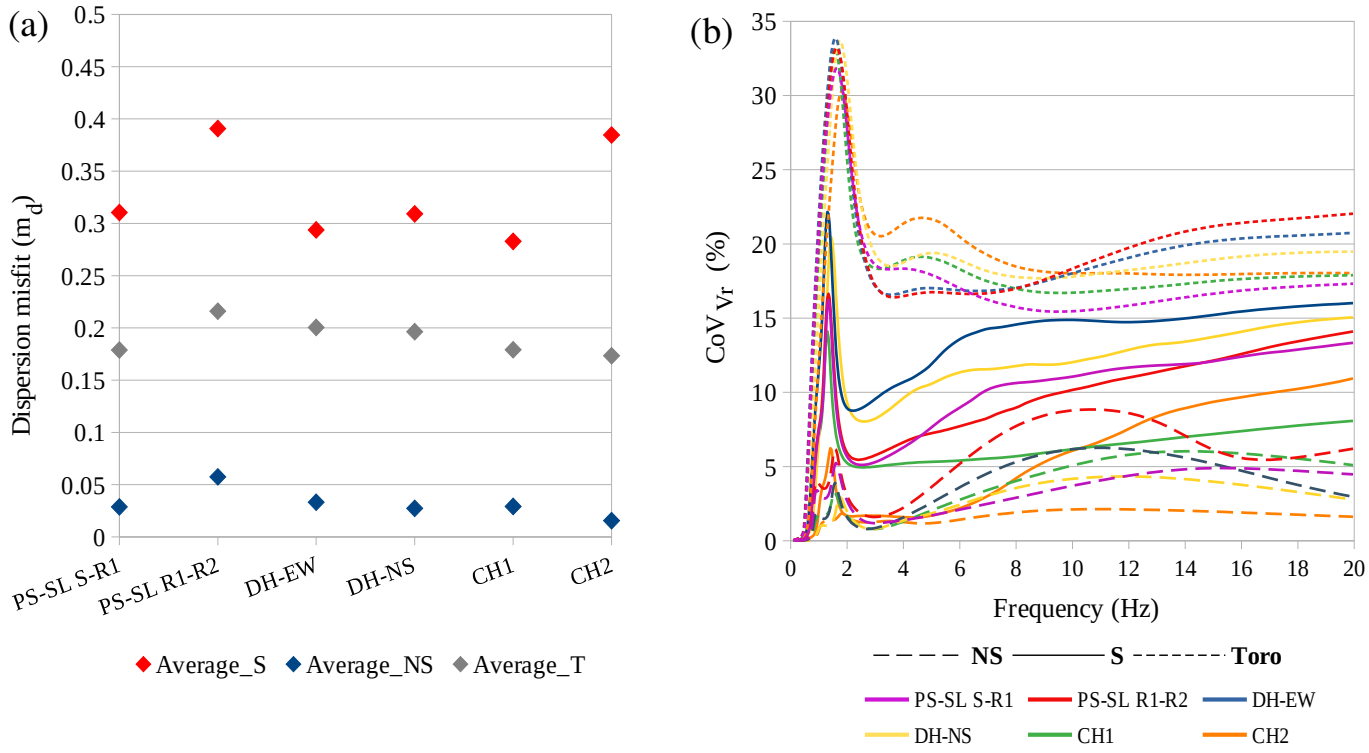

Fig. 6. (a) Average dispersion misfit (m_d) computed between pseudo-experimental DCs relative to each of the six base-case V_S profiles at Mirandola site and each realization of its corresponding 200 sets of theoretical DCs calculated from the nonstationary (in blue), stationary (in red) and the Toro (1995) (in grey) randomized V_S profiles; and (b) dispersion coefficient of variation (CoV_{Vr}) computed between each 200 sets of theoretical DCs calculated from the nonstationary (dashed line), stationary (continuous line), and the Toro (1995) (dotted line) randomized V_S profiles for the six base-case V_S profiles at Mirandola site.

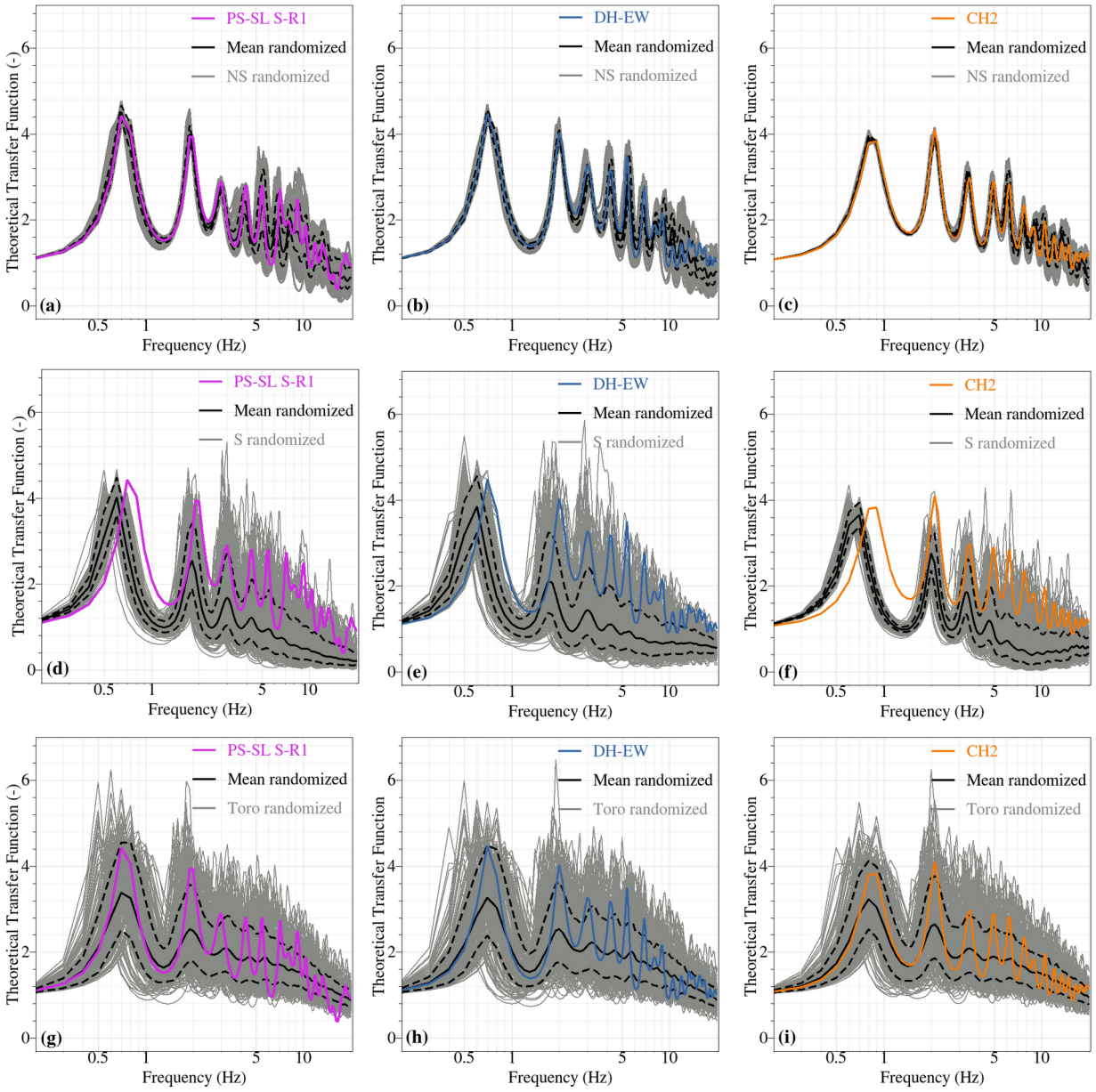

Fig. 7. The 200-sets of theoretical transfer functions calculated from (a-c) non-stationary; (d-f) stationary; and (g-i) Toro (1995) randomized profiles for three base-case V_S profiles alongside their mean randomized TTFs (solid black line) and related standard deviations ± 1σ (dotted black lines). Also shown in solid colored curves the pseudo-experimental TFs computed from the three base-case V_S profiles at Mirandola site.

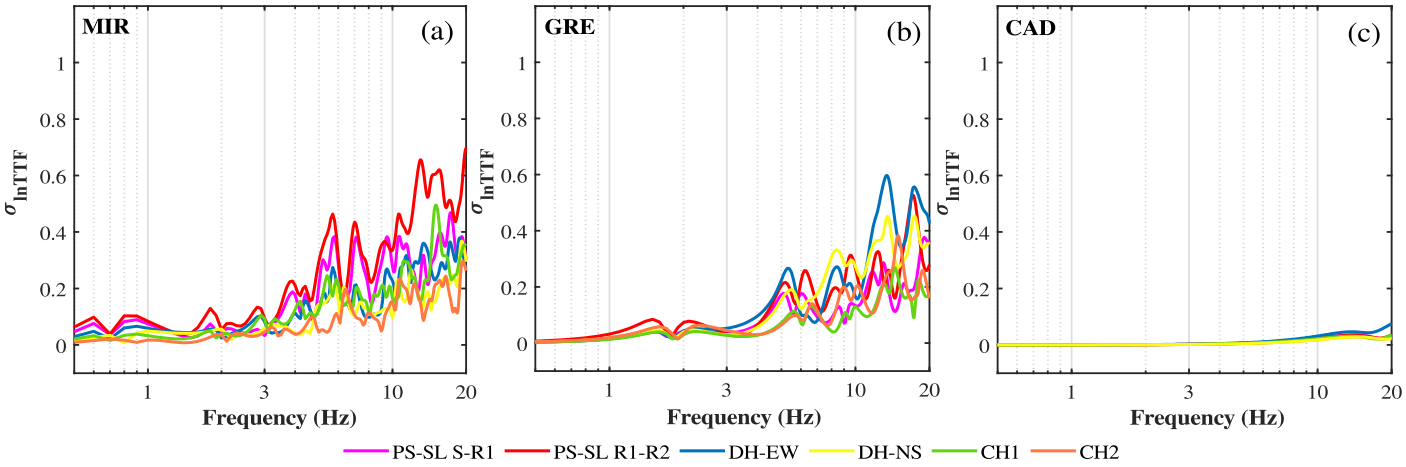

Fig. 8. Logarithmic standard deviations computed for the 200 sets of theoretical transfer functions calculated from nonstationary randomized V_S profiles for six base-case V_S profiles in Mirandola, Grenoble, and Cadarache sites.

Appendix S1: complementary results for Mirandola site

Figures

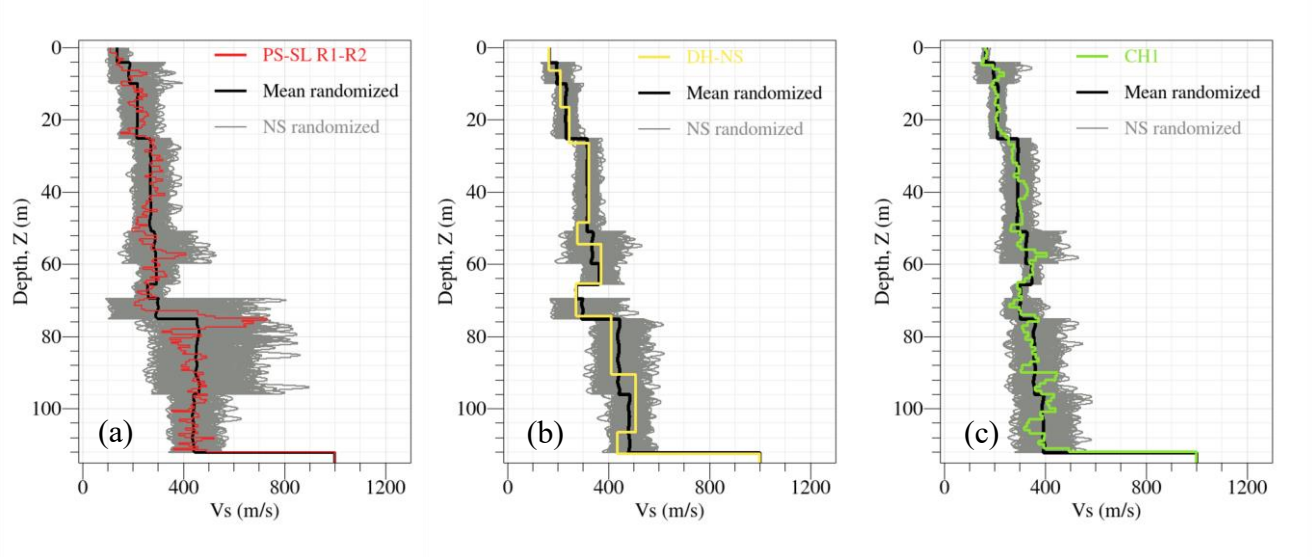

Fig. S1. Generated suites of 200 V_S profiles (grey curves) following the proposed non-stationary approach for three base-case V_S profiles at Mirandola: (a) PS-SL R1-R2; (b) DH-NS; and (c) CH1 alongside the average randomized profile (black curve). The invasively-measured base-case V_S profiles at Mirandola are indicated in color.

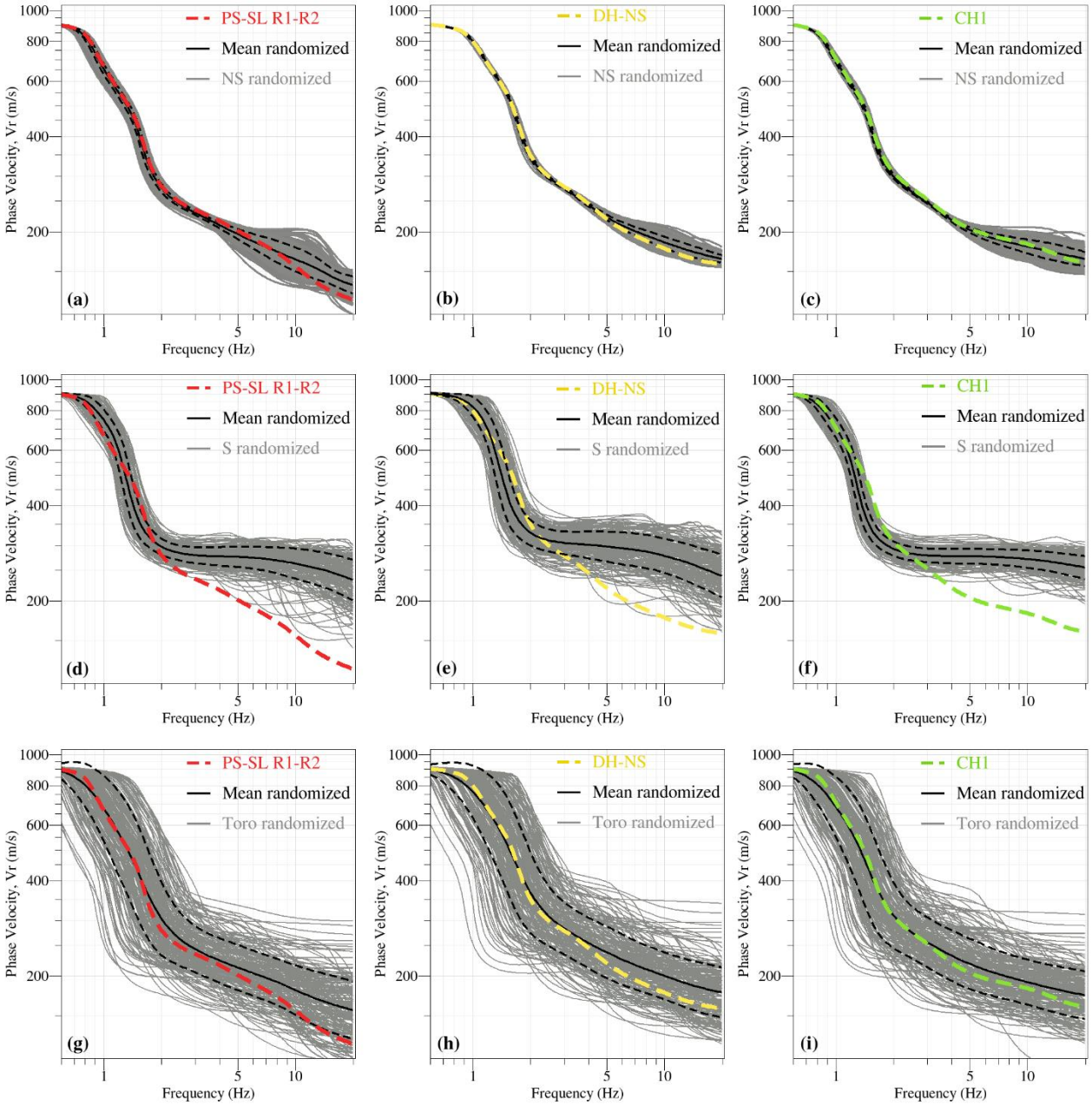

Fig. S2. The 200-sets of theoretical dispersion curves calculated from (a-c) non-stationary; (d-f) stationary; and (g-i) Toro (1995) randomized profiles for three base-case V_S profiles alongside their mean randomized TDCs (solid black line) and related standard deviations ± 1σ (dotted black lines). Also shown in colored curves the pseudo-experimental DCs computed from the three base-case V_S profiles at Mirandola site.

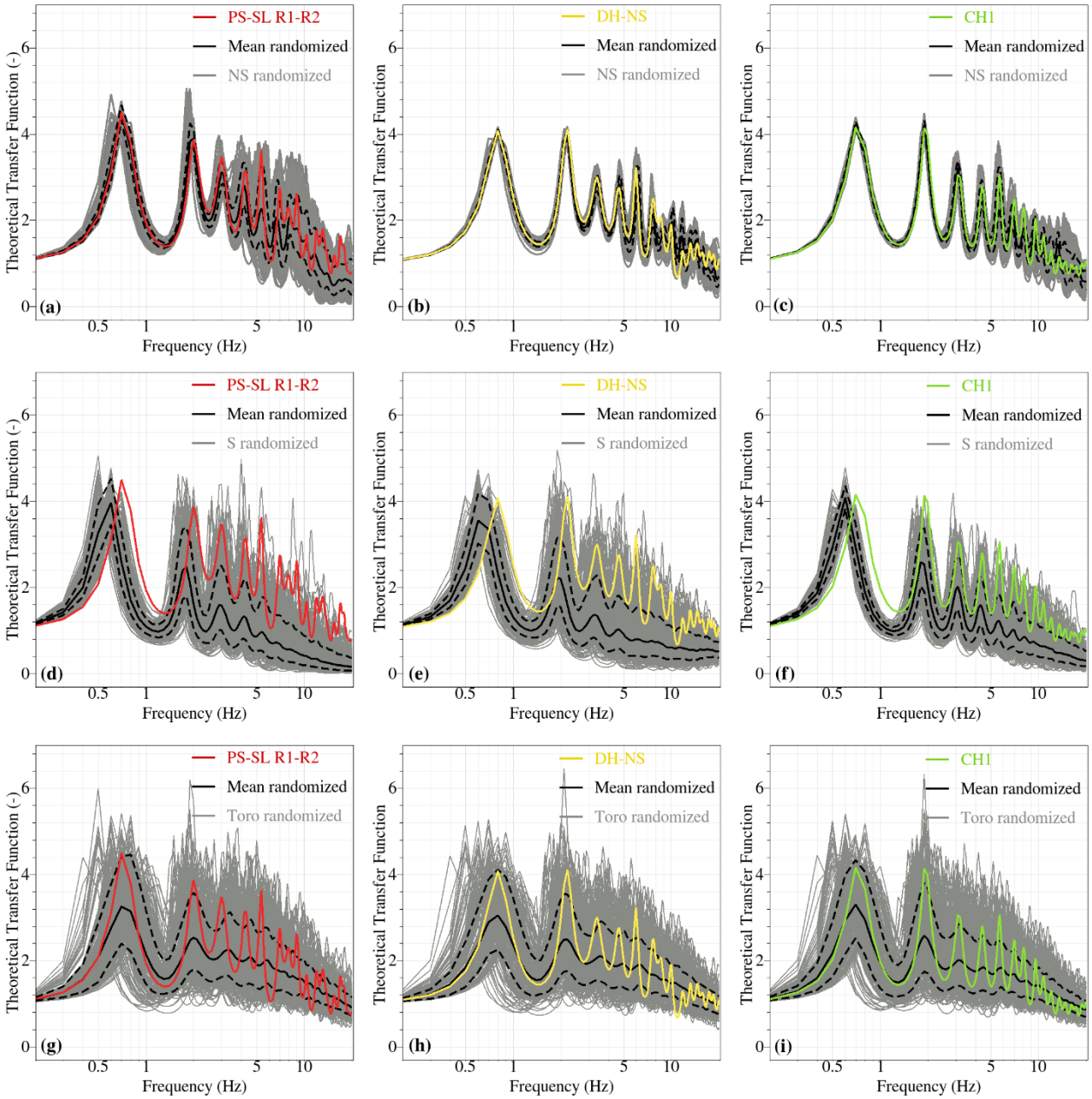

Fig. S3. The 200-sets of theoretical transfer functions calculated from (a-c) non-stationary; (d-f) stationary; and (g-i) Toro (1995) randomized profiles for three base-case V_S profiles alongside their mean randomized TTFs (solid black line) and related standard deviations ± 1σ (dotted black lines). Also shown in colored curves the pseudo-experimental TFs computed from the three base-case V_S profiles at Mirandola site.

Appendix S2: complementary results for Grenoble site

Tables

Table S1. Vertical scale of fluctuation θ (m) for each layer (layer numbering ordered from surface to depth) in the six base-case borehole V_S profiles in Grenoble site. Also shown are the average (μ) and CoV of θ for each layer.

Layer	Thickness (m)	Parameter	PS-SL S-R1	PS-SL R1-R2	DH-EW	DH-NS	CH1	CH2	$\mu_{(\theta)}$	$CoV_{(\theta)}$
1	6.5	$\boldsymbol{\theta_1}$	0.5	0.79	2.28	2.3	0.91	0.47	1.21	70.25
2	9	$\boldsymbol{\theta_2}$	0.66	0.4	0.83	0.83	1.05	1.2	0.83	33.73
3	2	$\boldsymbol{\theta_3}$	0.82	0.6	0.73	0.73	0.96	1	0.81	18.52
4	5	$\boldsymbol{\theta_4}$	1.41	1.47	1.03	1.03	1.03	1.01	1.16	18.97
5	3.5	$\boldsymbol{\theta_5}$	1.22	1.28	1.21	1.3	1.18	1.19	1.23	4.07
6	2	$\boldsymbol{\theta_6}$	0.8	0.32	0.7	0.7	0.59	0.54	0.61	27.87
7	5	$\boldsymbol{\theta_7}$	0.85	0.2	0.95	0.95	1.29	1.52	0.96	46.88
8	12	$\boldsymbol{\theta_8}$	3.65	1.44	1.14	3.22	2.55	2.55	2.43	40.33

Table S2. Coefficient of variation CoV_{Vs} (%) for each layer (layer numbering ordered from surface to depth) in the six base-case borehole V_S profiles in Grenoble site with the number of V_S samples indicated in parentheses for each layer. Also shown are the average (μ) and CoV of CoV_{Vs} for each layer.

Layer	Parameter	PS-SL S-R1	PS-SL R1-R2	DH-EW	DH-NS	CH1	CH2	$\mu_{(CoV)}$	$CoV_{(CoV)}$
1	$\boldsymbol{CoV_1}$	4.95(7)	10.05(10)	33.34(14)	31.68(14)	5.34(6)	6.52(6)	15.31	87.85
2	$\boldsymbol{CoV_2}$	15.31(19)	17.48(19)	0.01(19)	0.01(19)	8.21(10)	12.37(10)	9.23	76.81
3	$\boldsymbol{CoV_3}$	22.23(5)	20.69(5)	17.17(5)	20.79(5)	11.36(3)	5.42(3)	16.28	40.60
4	$\boldsymbol{CoV_4}$	17.87(11)	19.33(11)	13.02(11)	15.12(11)	12.72(7)	8.44(7)	14.42	27.25
5	$\boldsymbol{CoV_5}$	11.08(8)	25.87(8)	21.50(8)	23.58(8)	24.84(4)	30.39(4)	22.88	28.37
6	$\boldsymbol{CoV_6}$	3.78(5)	8.38(5)	0.01(5)	0.01(5)	3.52(3)	1.28(3)	3.16	90.19
7	$\boldsymbol{CoV_7}$	2.08(11)	7.13(11)	0.01(11)	0.01(11)	3.02(6)	2.12(6)	2.73	83.88
8	$\boldsymbol{CoV_8}$	10.83(25)	12.11(25)	12.71(25)	12.57(25)	9.35(13)	9.87(13)	11.24	12.72

Table S3. Average determination coefficient Q^2 for the leave-one-out cross-validation error and average Pearson's sample correlation coefficient r_p over the 200-sets of non-stationary, stationary and Toro's (1995) theoretical transfer functions (TTFs) for six base-case profiles compared to corresponding pseudo-experimental transfer functions for Grenoble site.

V_S profile	Q^2			r_P		
Grenoble	Non-stationary	Stationary	Toro (1995)	Non-stationary	Stationary	Toro (1995)
PS-SL S-R1	0.942	0.835	0.837	0.897	0.599	0.453
PS-SL R1-R2	0.875	0.766	0.739	0.862	0.598	0.452
DH-EW	0.764	0.608	0.721	0.592	0.331	0.309
DH-NS	0.830	0.682	0.761	0.646	0.369	0.330
CH1	0.964	0.841	0.829	0.925	0.569	0.429
CH2	0.963	0.869	0.852	0.897	0.569	0.436

Figures

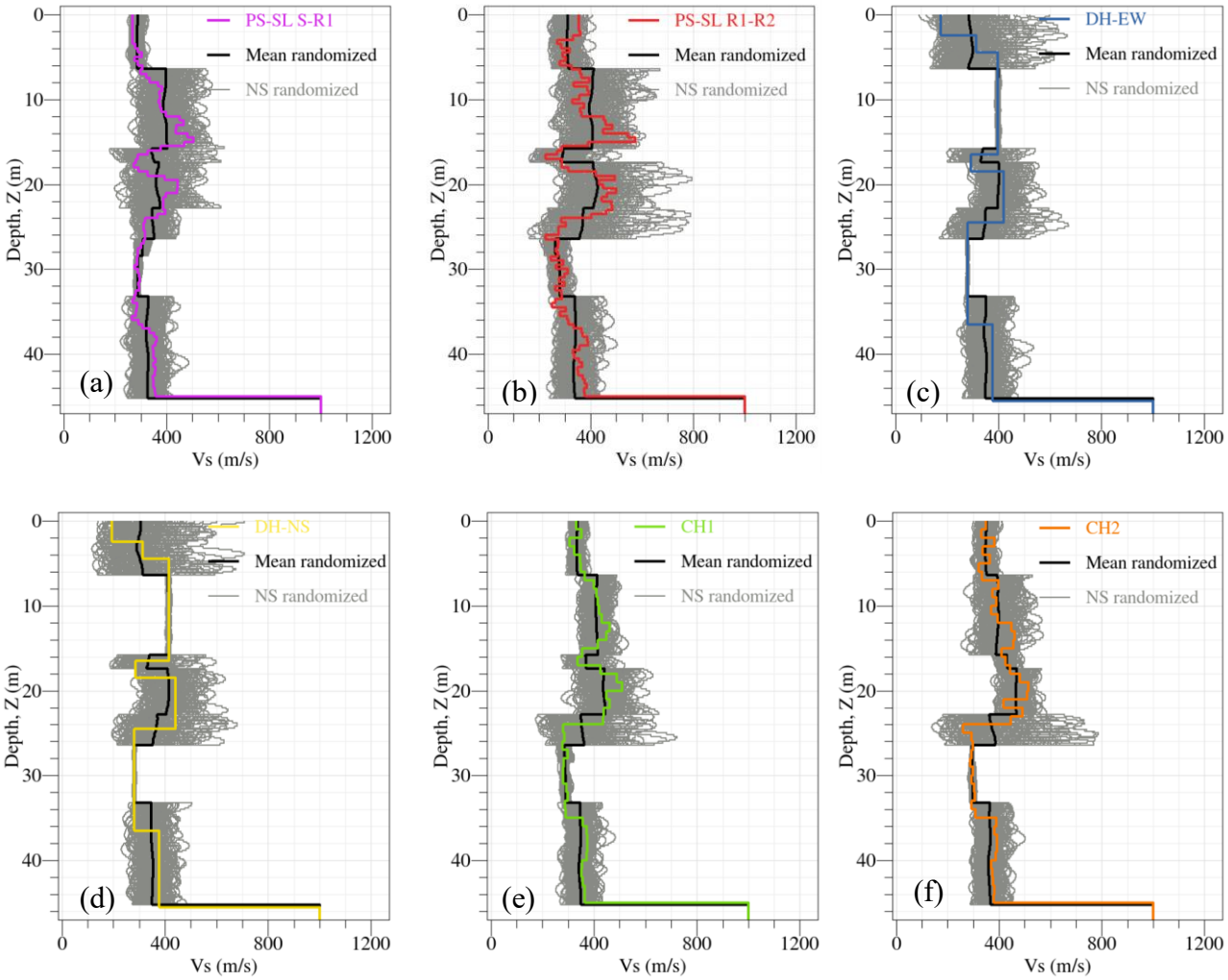

Fig. S4. Generated suites of 200 V_S profiles (grey curves) following the proposed non-stationary approach for six base-case V_S profiles at Grenoble: (a) PS-SL S-R1; (b) PS-SL R1-R2; (c) DH-EW; (d) DH-NS; (e) CH1; and (f) CH2) alongside the average randomized profile (black curve). The invasively-measured base-case V_S profiles at Grenoble are indicated in color.

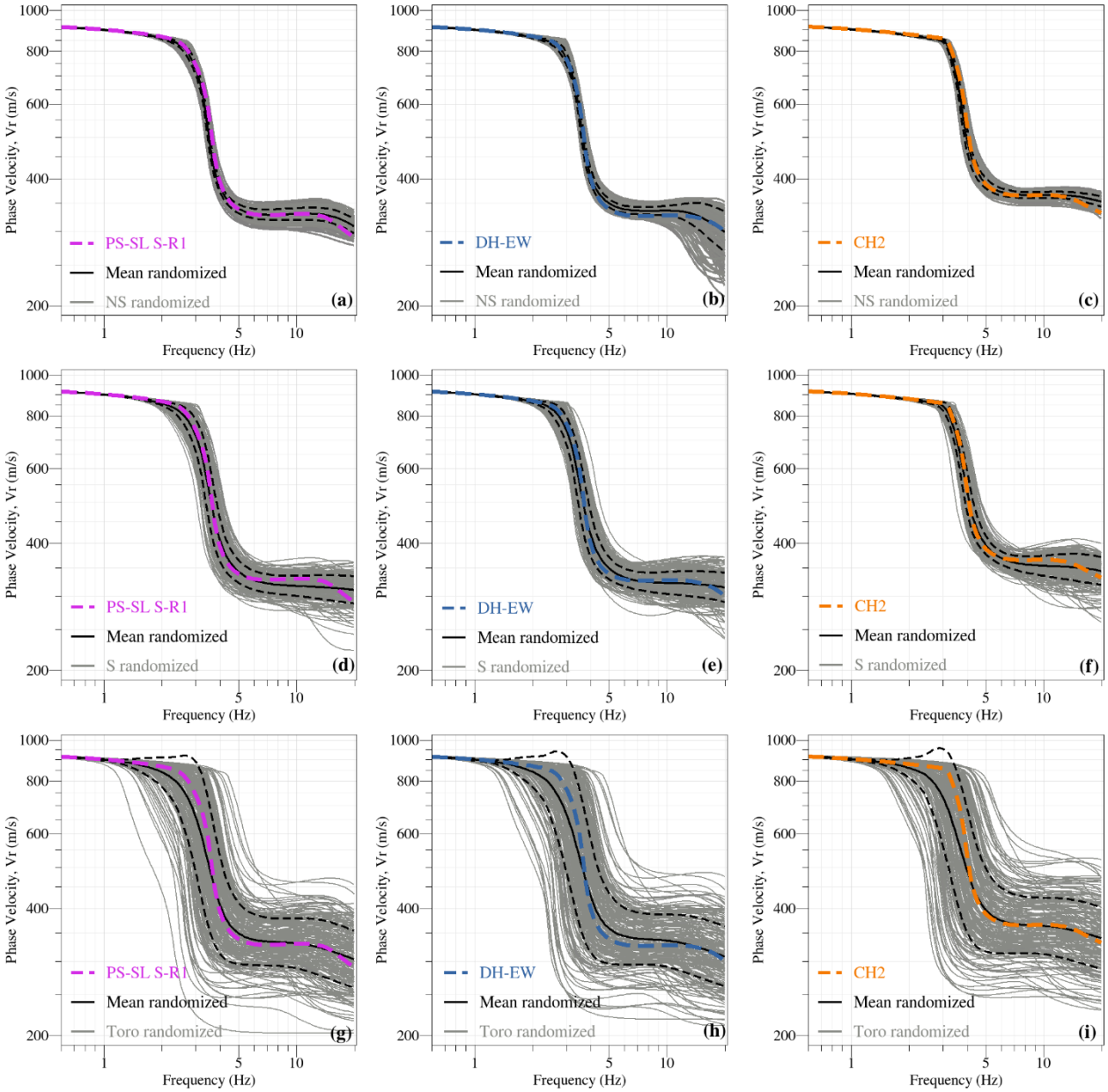

Fig. S5. The 200-sets of theoretical dispersion curves calculated from (a-c) non-stationary; (d-f) stationary; and (g-i) Toro (1995) randomized profiles for six base-case V_S profiles alongside their mean randomized TDCs (solid black line) and related standard deviations ± 1σ (dotted black lines). Also shown in colored curves the pseudo-experimental DCs computed from the three base-case V_S profiles at Grenoble site.

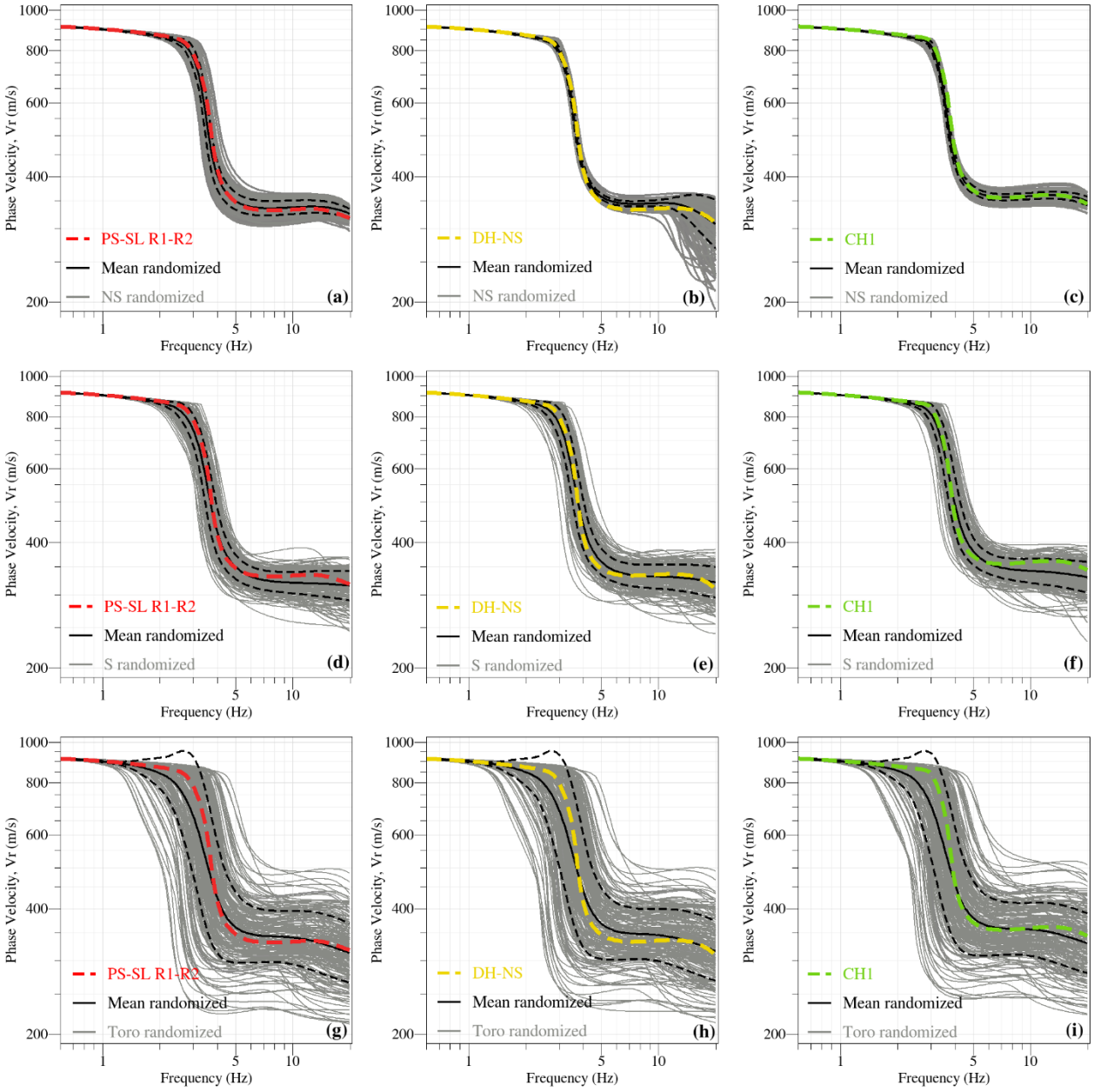

Fig. S5. Continued.

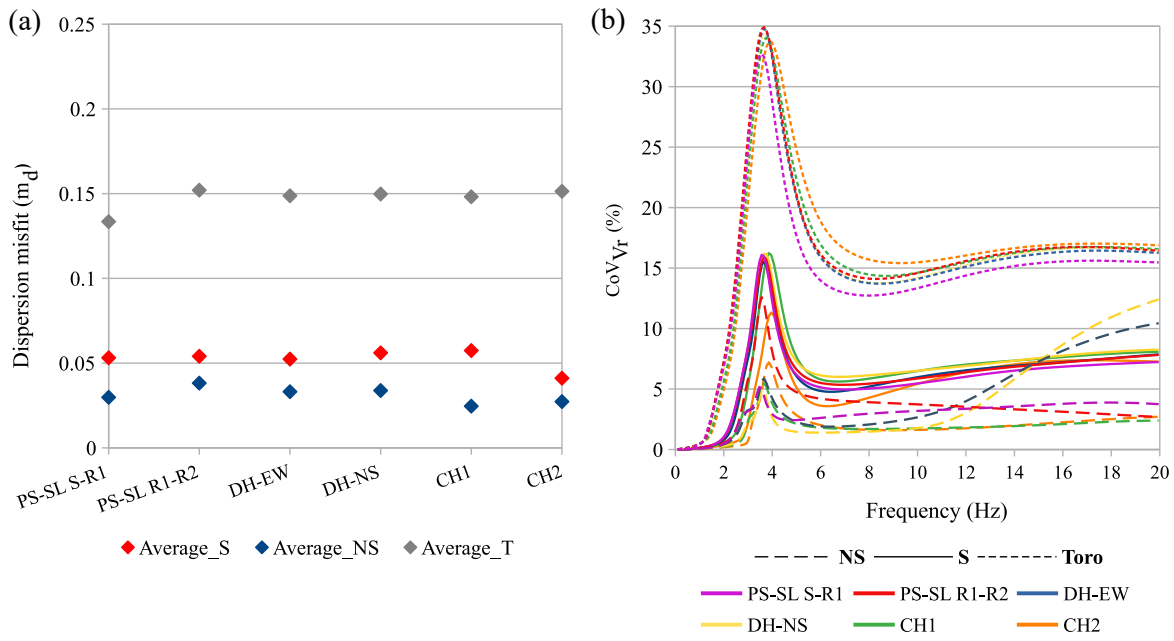

Fig. S6. (a) Average dispersion misfit (m_d) computed between pseudo-experimental DCs relative to each of the six base-case V_S profiles at Grenoble site and each realization of its corresponding 200 sets of theoretical DCs calculated from the non-stationary (in blue), stationary (in red) and Toro (1995) (in grey) randomized V_S profiles; and (b) dispersion coefficient of variation (CoV_{Vr}) computed between each 200-sets of theoretical DCs calculated from the non-stationary (dashed line), stationary (continuous line) and Toro (1995) (dotted line) randomized V_S profiles for the six base-case V_S profiles at Grenoble site.

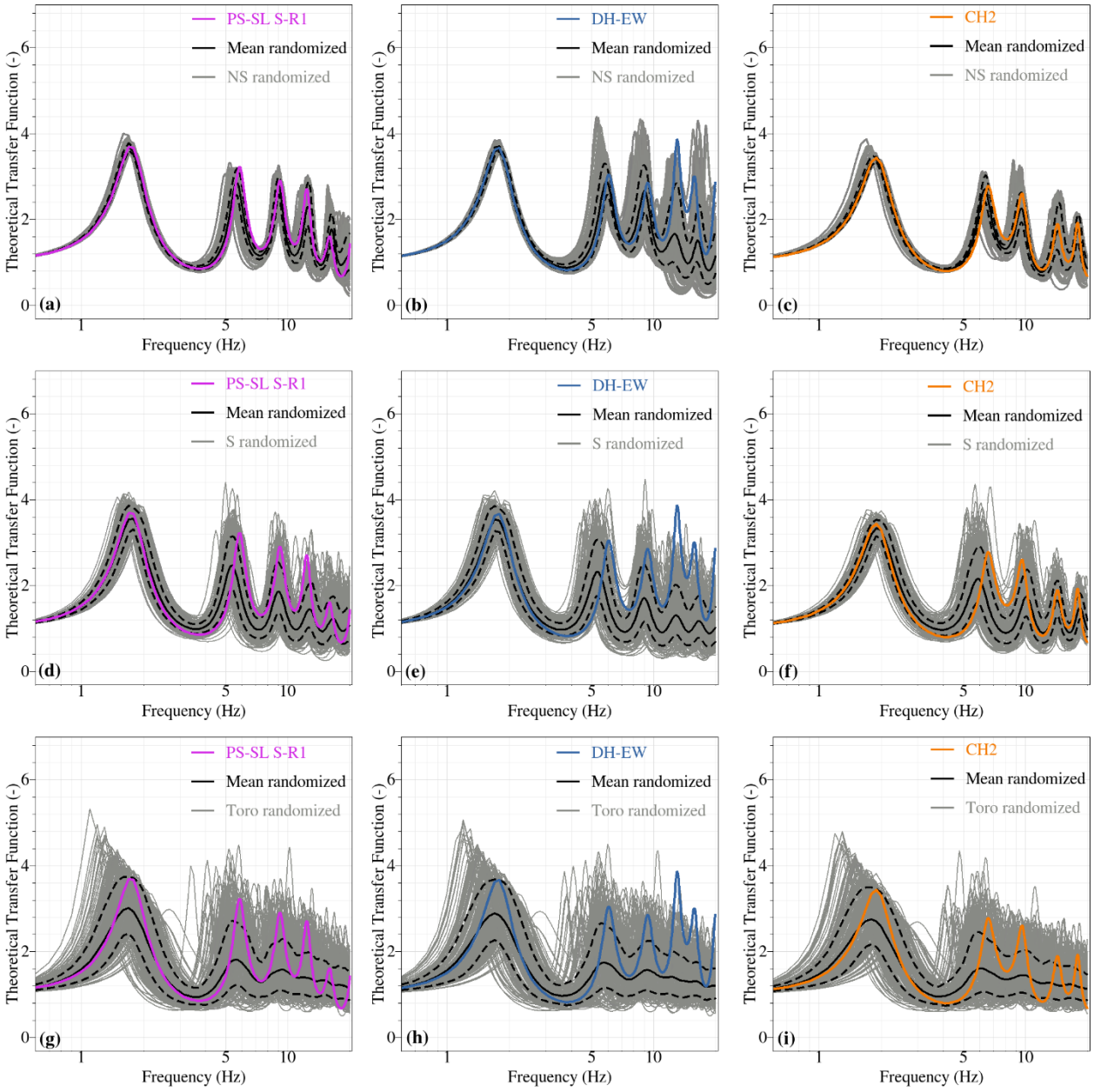

Fig. S7. The 200-sets of theoretical transfer functions calculated from (a-c) non-stationary; (d-f) stationary; and (g-i) Toro (1995) randomized profiles for six base-case V_S profiles alongside their mean randomized TTFs (solid black line) and related standard deviations ± 1σ (dotted black lines). Also shown in colored curves the pseudo-experimental TFs computed from the six base-case V_S profiles at Grenoble site.

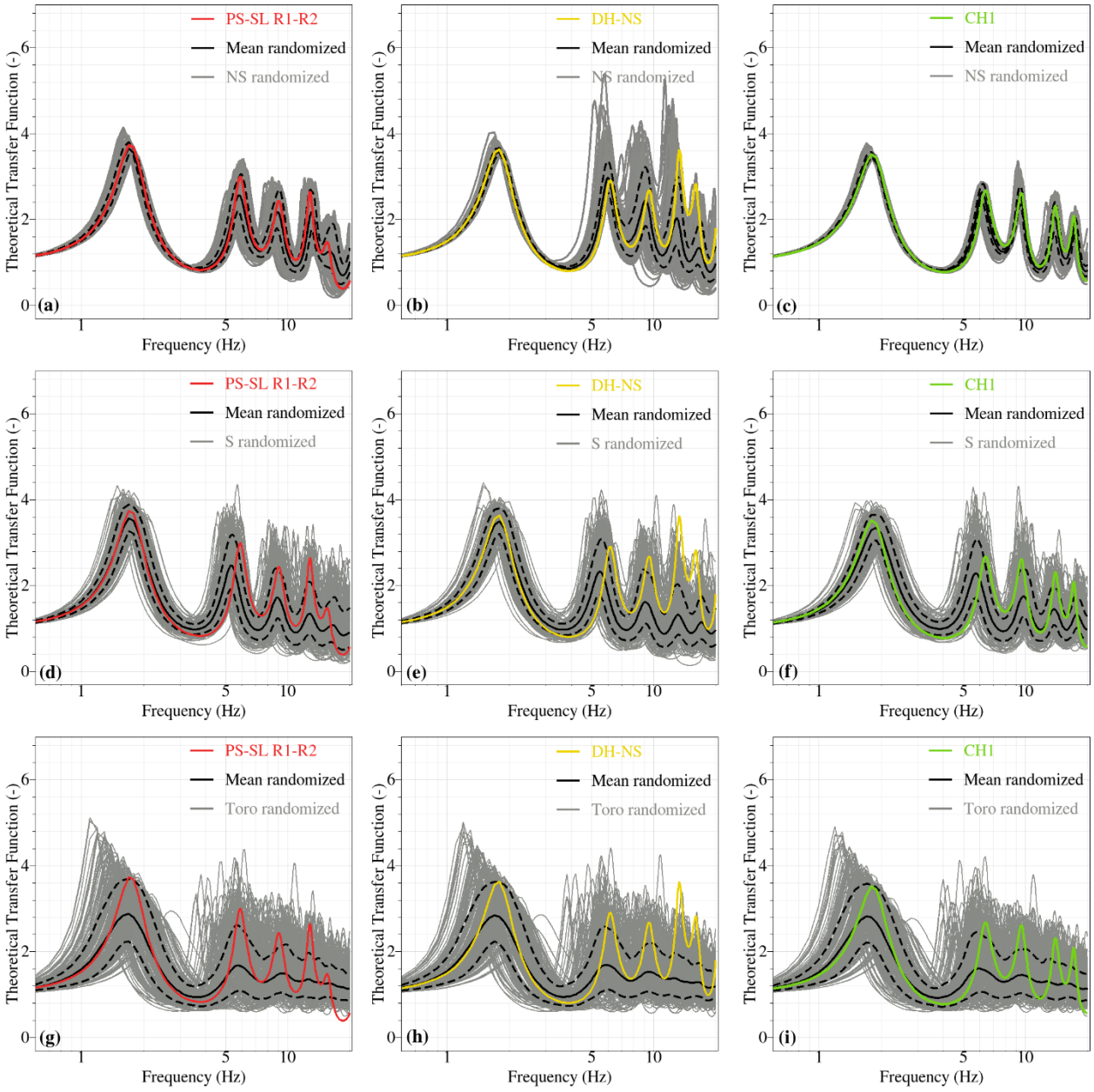

Fig. S7. Continued.

Appendix S3: complementary results for Cadarache site

Tables

Table S4. Vertical scale of fluctuation θ (m) for each layer (layer numbering ordered from surface to depth) in the six base-case borehole V_S profiles in Cadarache site. Also shown are the average (μ) and CoV of θ for each layer.

Layer	Thickness (m)	Parameter	PS-SL S-R1	PS-SL R1-R2	DH	DH-NS	CH1	CH2	$\mu_{(\theta)}$	$CoV_{(\theta)}$
1	4	$\boldsymbol{\theta_1}$	0.48	0.62	0.46	1.36	0.92	0.81	0.78	43.59
2	21	$\boldsymbol{\theta_2}$	1.76	1.24	1.54	1.39	2.13	2.02	1.68	20.83
3	1.5	$\boldsymbol{\theta_3}$	0.41	0.58	0.47	0.59	0.97	0.54	0.59	33.89
4	4.5	$\boldsymbol{\theta_4}$	0.83	0.58	0.47	0.77	0.99	0.97	0.77	27.27

Table S5. Coefficient of variation CoV_{Vs} (%) for each layer (layer numbering ordered from surface to depth) in the six base-case borehole V_S profiles in Cadarache site with the number of V_S samples indicated in parentheses for each layer. Also shown are the average (μ) and CoV of CoV_{Vs} for each layer.

Layer	Parameter	PS-SL S-R1	PS-SL R1-R2	DH	DH-NS	CH1	CH2	$\mu_{(CoV)}$	$CoV_{(CoV)}$
1	$\boldsymbol{CoV_1}$	3.34(3)	6.93(6)	12.21(9)	10.17(9)	8.04(3)	12.77(3)	8.91	39.86
2	$\boldsymbol{CoV_2}$	25.39(43)	27.50(43)	25.13(43)	25.31(43)	20.39(22)	22.25(22)	24.33	10.50
3	$\boldsymbol{CoV_3}$	1.37(4)	6.80(4)	4.30(4)	0.01(4)	7.56(3)	4.94(3)	4.16	71.39
4	$\boldsymbol{CoV_4}$	8.01(10)	6.82(10)	0.01(10)	0.01(10)	12.97(5)	8.98(5)	6.13	84.35

Table S6. Average determination coefficient Q^2 for the leave-one-out cross-validation error and average Pearson's sample correlation coefficient r_p over the 200-sets of non-stationary, stationary and Toro's (1995) theoretical transfer functions (TTFs) for six base-case profiles compared to corresponding pseudo-experimental transfer functions for Cadarache site.

V_S profile	Q^2			r_P		
Cadarache	Non-stationary	Stationary	Toro (1995)	Non-stationary	Stationary	Toro (1995)
PS-SL S-R1	0.999	0.995	0.997	0.983	0.921	0.956
PS-SL R1-R2	0.999	0.992	0.997	0.983	0.868	0.958
DH	0.995	0.919	0.992	0.966	0.458	0.942
DH-NS	0.999	0.989	0.998	0.989	0.824	0.966
CH1	0.999	0.997	0.997	0.985	0.938	0.952
CH2	0.999	0.994	0.997	0.986	0.889	0.949

Figures

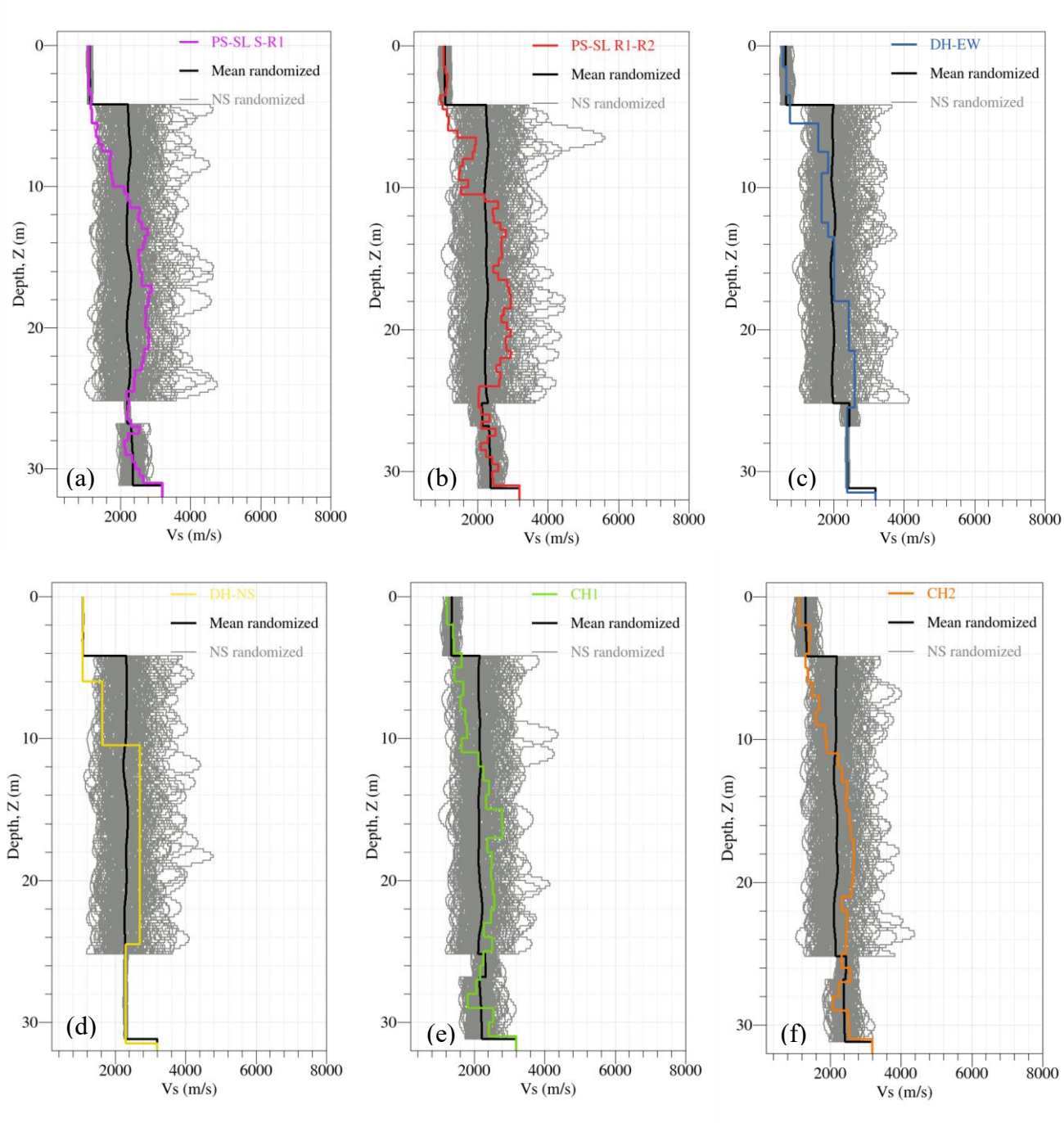

Fig. S8. Generated suites of 200 V_S profiles (grey curves) following the proposed non-stationary approach for three base-case V_S profiles at Cadarache: (a) PS-SL S-R1; (b) PS-SL R1-R2; (c) DH-EW; (d) DH-NS; (e) CH1; and (f) CH2 alongside the average randomized profile (black curve). The invasively-measured base-case V_S profiles at Cadarache are indicated in color.

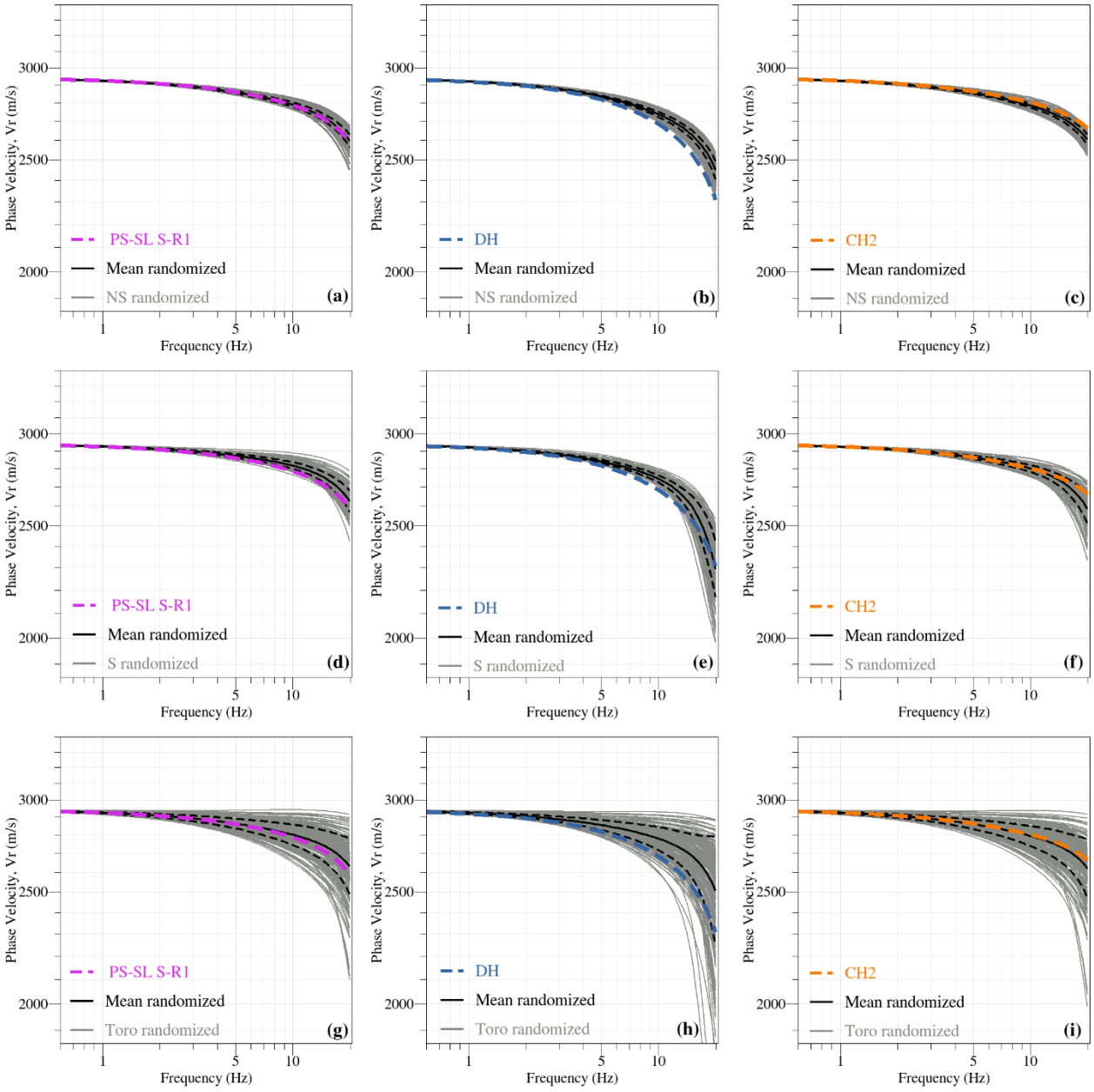

Fig. S9. The 200-sets of theoretical dispersion curves calculated from (a-c) non-stationary; (d-f) stationary; and (g-i) Toro (1995) randomized profiles for six base-case V_S profiles alongside their mean randomized TDCs (solid black line) and related standard deviations ± 1σ (dotted black lines). Also shown in colored curves the pseudo-experimental DCs computed from the three base-case V_S profiles at Cadarache site.

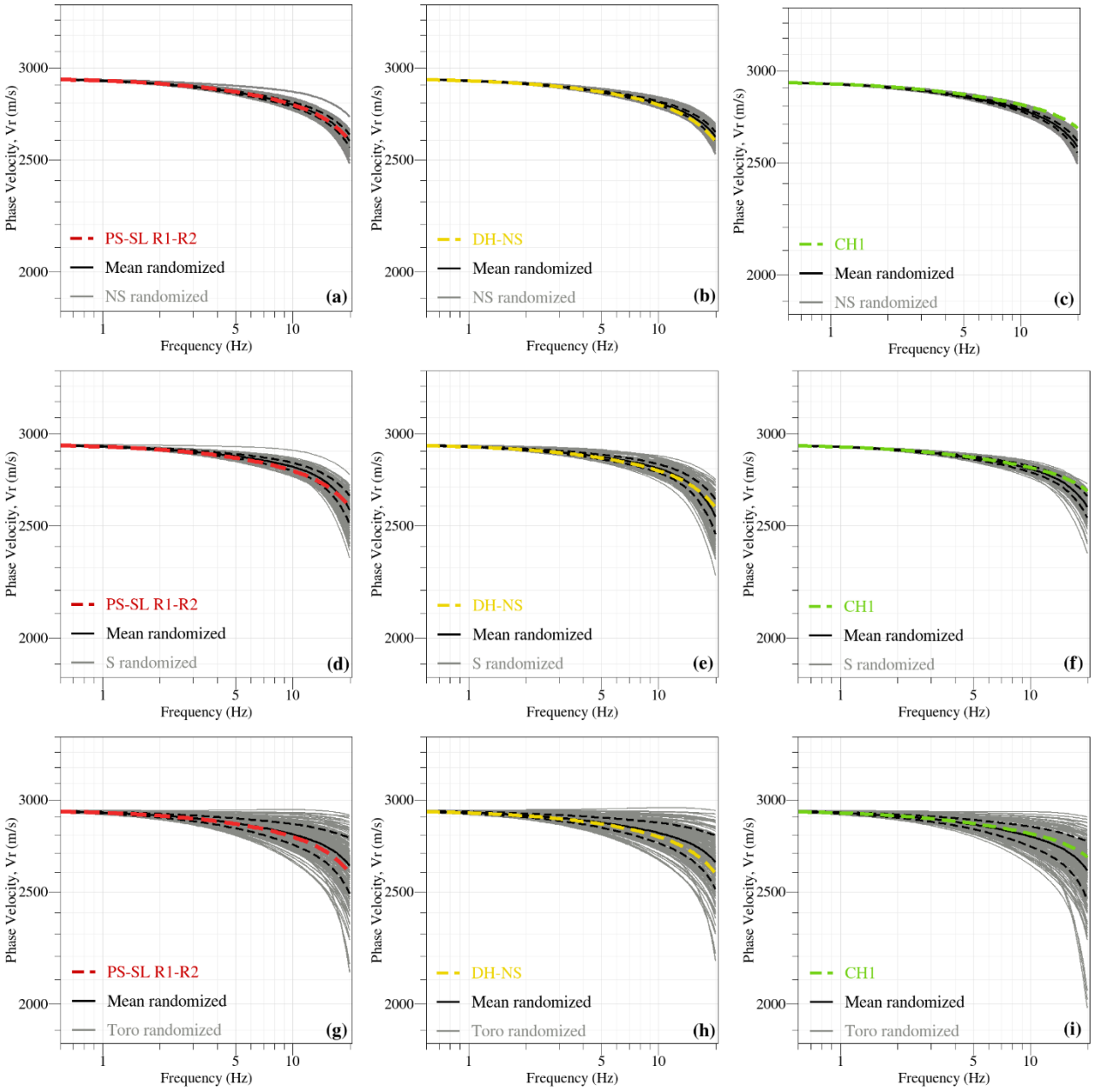

Fig. S9. Continued.

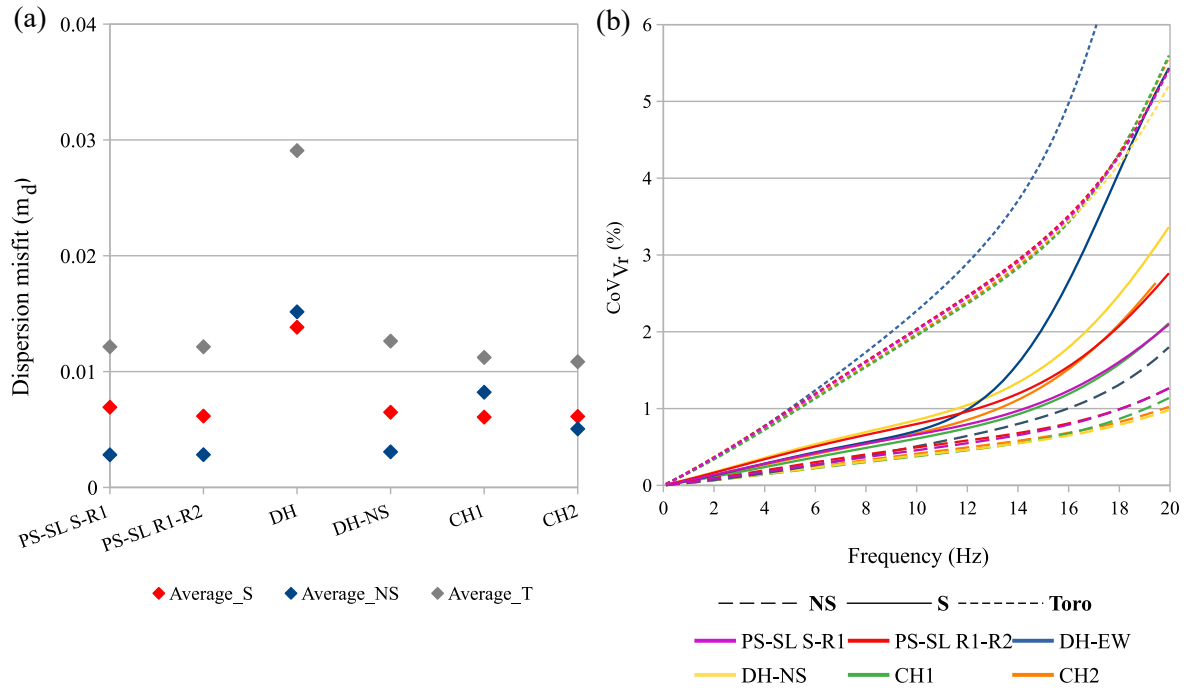

Fig. S10. (a) Average dispersion misfit (m_d) computed between pseudo-experimental DCs relative to each of the six base-case V_S profiles at Cadarache site and each realization of its corresponding 200 sets of theoretical DCs calculated from the non-stationary (in blue), stationary (in red) and Toro's (1995) (in grey) randomized V_S profiles; and (b) dispersion coefficient of variation (CoV_{Vr}) computed between each 200-sets of theoretical DCs calculated from the non-stationary (dashed line), stationary (continuous line) and Toro's (1995) (dotted line) randomized V_S profiles for the six base-case V_S profiles at Cadarache site.

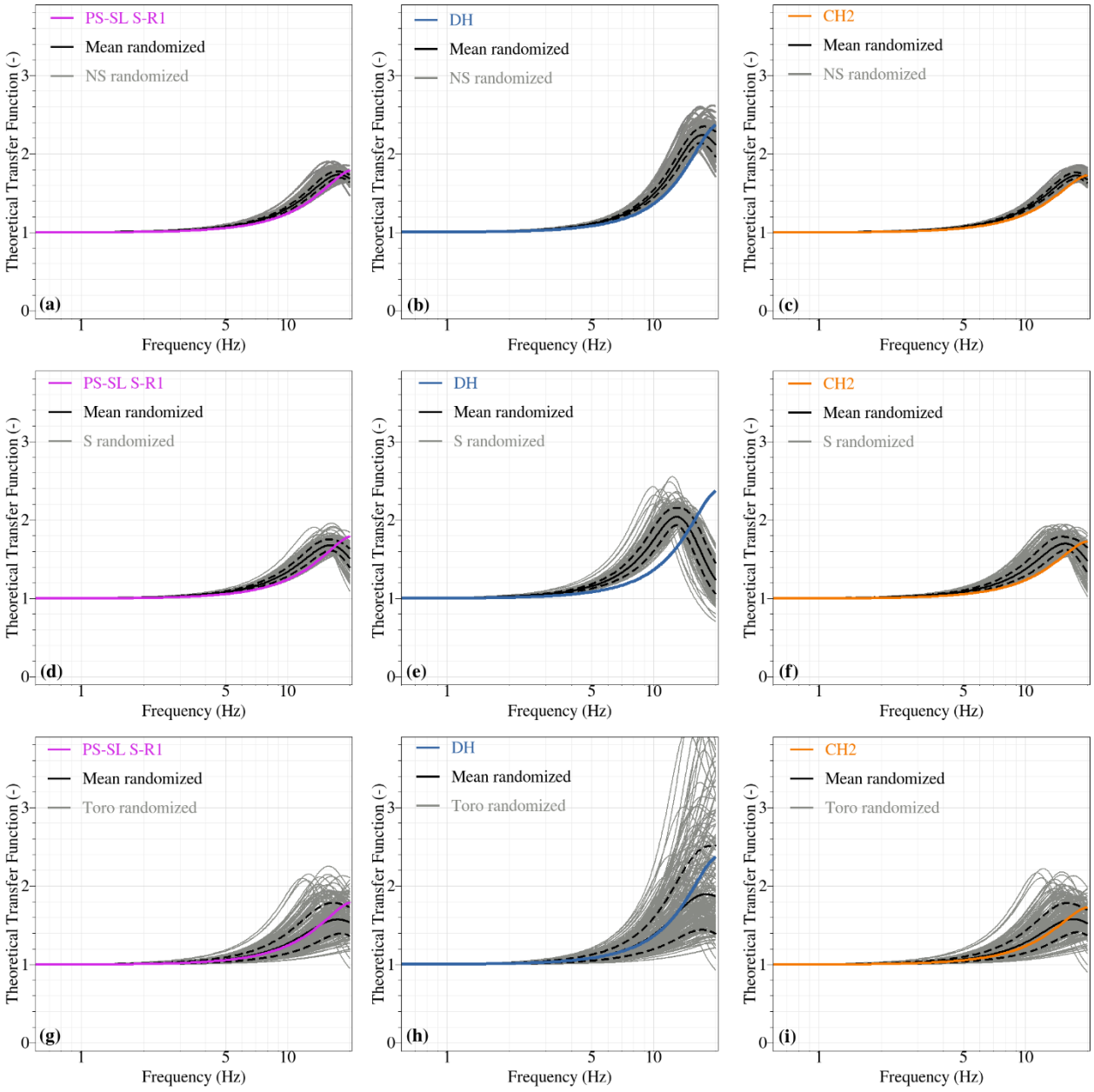

Fig. S11. The 200-sets of theoretical transfer functions calculated from (a-c) non-stationary; (d-f) stationary; and (g-i) Toro (1995) randomized profiles for six base-case V_S profiles alongside their mean randomized TTFs (solid black line) and related standard deviations ± 1σ (dotted black lines). Also shown in colored curves the pseudo-experimental TFs computed from the six base-case V_S profiles at Cadarache site.

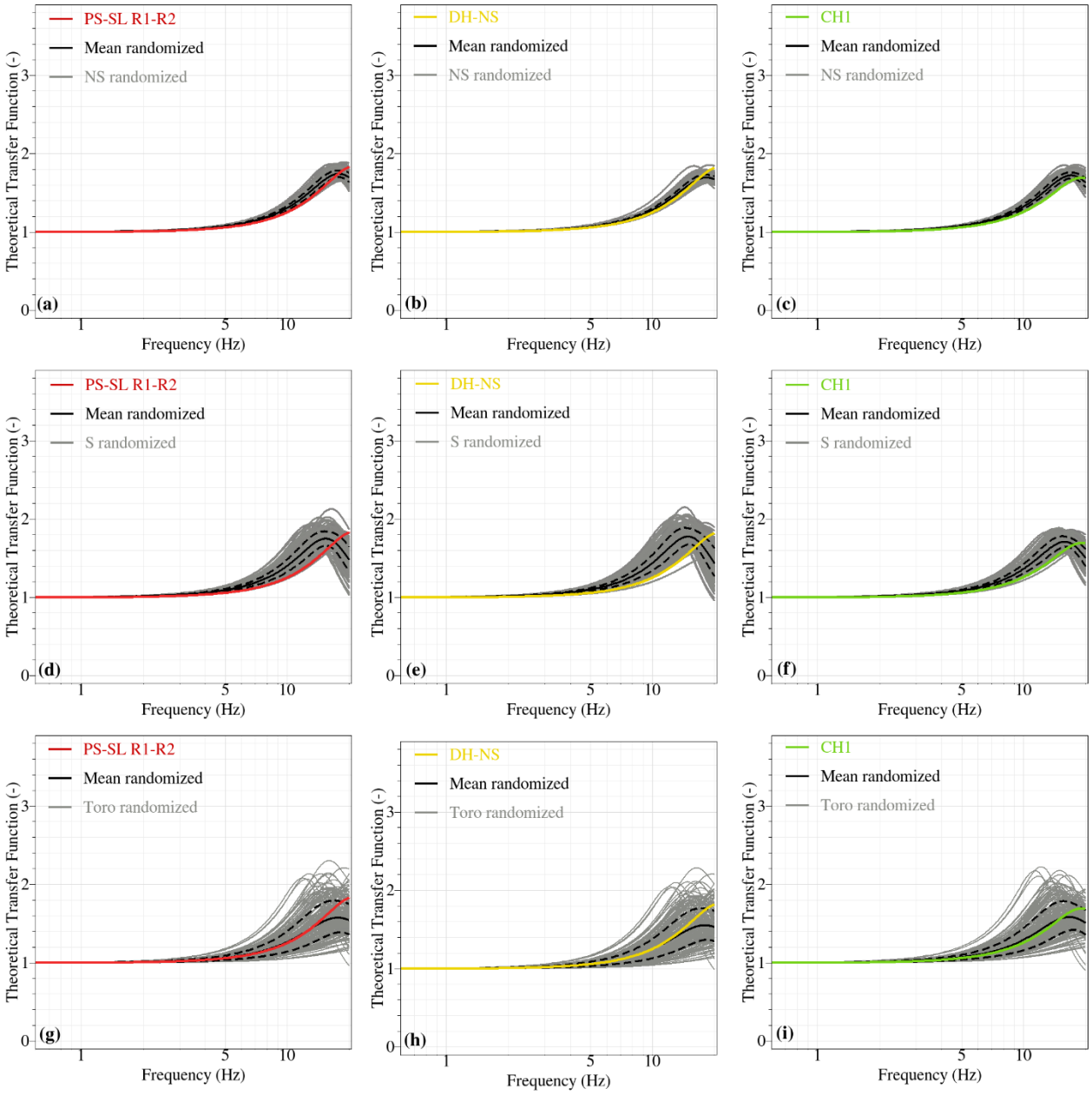

Fig. S11. Continued.

Appendix S4: V_S variability quantification parameters for base-case profiles

Tables

Table S7. Quantification parameters used for stationary V_S randomization for the six base-case V_S profiles at each of the three sites. μ_{Vs} is the average V_S, CoV_{Vs} is the coefficient of variation and θ is the vertical scale of fluctuation.

Mirandola	PS-SL S-R1	PS-SL R1-R2	DH-EW	DH-NS	CH1	CH2
μ_{Vs} (m/s)	318	319	310	341	305	346
CoV_{Vs} (%)	33	35	31	30	24	28
θ (m)	4.8	4.3	8.8	9.3	5.4	4.2

Grenoble	PS-SL S-R1	PS-SL R1-R2	DH-EW	DH-NS	CH1	CH2
μ_{Vs} (m/s)	341	349	345	353	366	376
CoV_{Vs} (%)	17	22	20	20	17	17
θ (m)	4.8	3.6	4.5	4.6	6.4	6.3

Cadarache	PS-SL S-R1	PS-SL R1-R2	DH	DH-NS	CH1	CH2
μ_{Vs} (m/s)	2224	2179	1898	2153	2118	2153
CoV_{Vs} (%)	25	29	35	29	21	23
θ (m)	2.2	2.0	2.2	2.6	2.2	3.1

Appendix S5: modifications to the Toro (1995) model components

The layering and velocity randomization models were implemented for the Toro (1995) approach applied in this paper without implementing the bedrock depth randomization. Therefore, this appendix presents an evaluation of the potential implications of these components (layering, velocity, and bedrock depth randomization) on the expected output variability. For this reason, a new set of Toro (1995) randomization was implemented by (1) fixing the layer thicknesses as the non-stationary approach and (2) varying the bedrock depth as the original Toro (1995) approach. The results of these two applications in terms of randomized V_S profiles and corresponding theoretical dispersion curves (TDCs) and theoretical transfer functions (TTFs) are presented in Figure S12 for the PS-SL S-R1 test at the MIR site.

The results provided by this application highlight minor differences in the variability of the Toro randomized V_S profiles and their ability to generate sets of consistent site signatures. In the case of constant layering, both the dispersion misfit m_d (average 0.14) and the CoV_{Vr} (maximum of 28.3%) slightly decrease compared to the case of variable layers thicknesses (average m_d of 0.18; maximum CoV_{Vr} of 31.8%). This decrease is caused by the randomized V_S being less variable with the constant layering that affects the values of V_S at the mid-depth of each layer. As a result, the mean randomized DC better fits the pseudo-EDC based on the base-case PS-SL S-R1 test. Additionally, the mean randomized TTF is slightly better aligned with the pseudo-Experimental transfer function (pseudo-ETF) (cross-validation error estimator $Q^2 = 0.858$; Pearson's correlation coefficient $r_P = 0.459$).

When applying the complete Toro (1995) model (i.e., the 3 models including V_S randomization, layering randomization, and bedrock depth and velocity randomization), the values of the dispersion misfit m_d (average 0.19) and the dispersion CoV_{Vr} (maximum of 35.6%) are slightly larger caused by the higher dispersion in the randomized DCs compared to the initial application of Toro (1995) (i.e., without bedrock variation). In addition, both the TTFs Q^2 of 0.832 and the r_P of 0.411 are slightly lower because of some minor extreme TTFs that are badly aligned with the site's resonance frequencies.

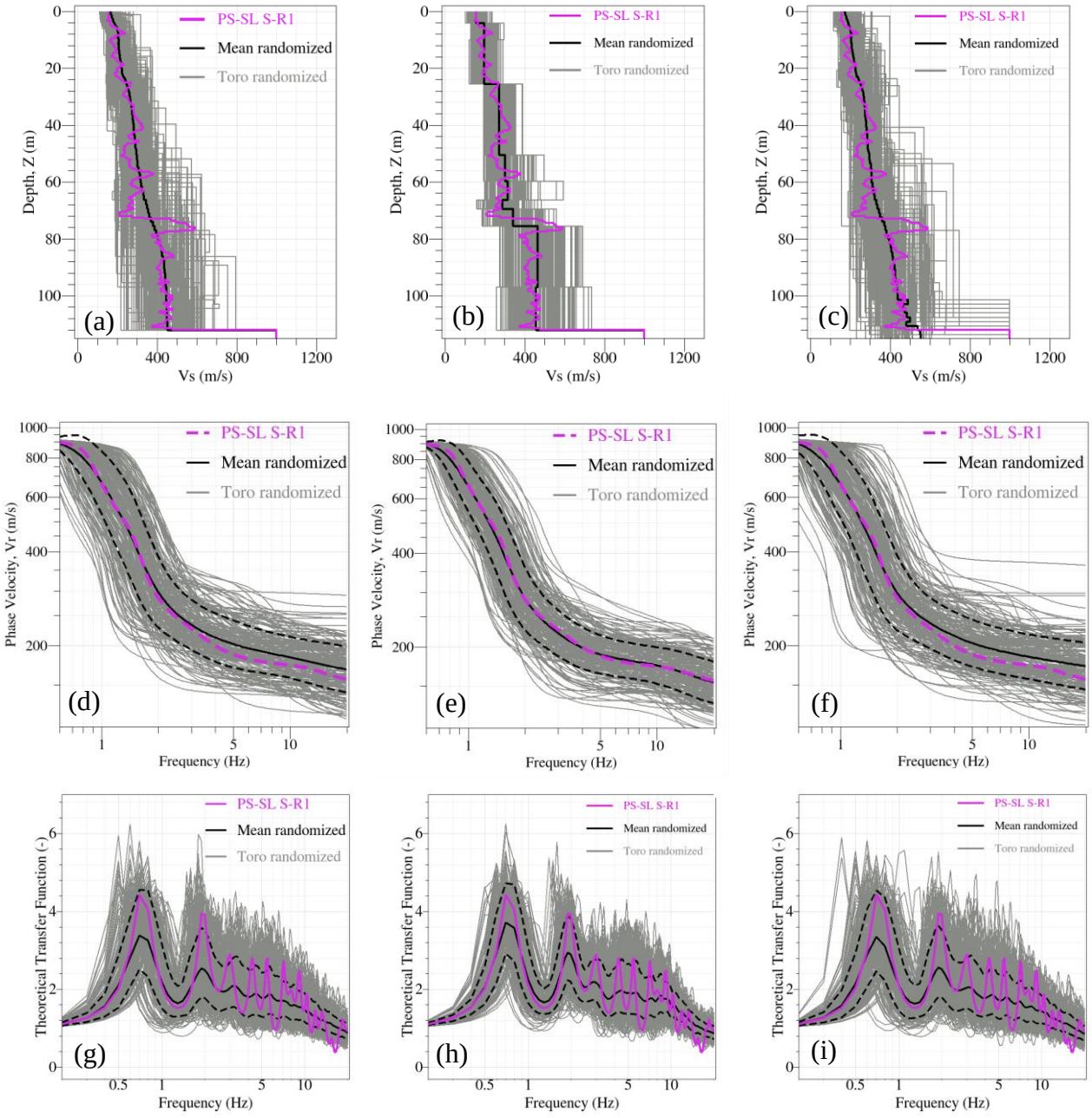

Fig. S12. Generated suites of 200 V_S profiles (a-c) following the Toro (1995) approach for PS-SL S-R1 base-case V_S profile at Mirandola indicated in magenta color, corresponding 200 sets of theoretical dispersion curves (d-f) and theoretical transfer functions (g- i) assuming velocity and layering randomization (a, d, g) velocity randomization (b, e, h) and velocity, layering and bedrock depth randomization (c, f, i) following the Toro (1995) model components.

In this paper, the application of the Toro (1995) randomization approach followed the instructions proposed by Toro (1995, 2022) as is done in practice. The choice of variability introduced to randomize V_S in soil layers, σ_{lnVs}, was made based on (i) the recommendations of Stewart et al. (2014) (Table 3 in the paper) when giving instructions on the Toro (1995) method application and (ii) the recent publications discussing the Toro (1995) application (e.g. Rathje et al. 2010; Teague et al. 2018; Passeri et al. 2020).

However, to investigate the impact of using a recommended σ_{lnVs} instead of a site-specific σ_{lnVs} on the set of Toro randomized V_S profiles, we have run a separate set of simulations using the site-specific vertical σ_{lnVs} computed from the individual soil layers in the base-case V_S profiles (same σ_{lnVs} used for non-stationary method application). In this appendix, we show an example for a DH base-case V_S profile (DH-EW) in the Grenoble site, because the base-case V_S profile exhibits both low and high levels of CoV_{Vs} (σ_{lnVs}) in individual soil layers. Instead of a fixed σ_{lnVs} at 0.15 (Table 3 in the paper), σ_{lnVs} is now variable with values between 0.05 and 0.16 depending on the layers (Table S8). The results of this application in terms of randomized V_S profiles and corresponding theoretical dispersion curves (TDCs) and theoretical transfer functions (TTFs) are presented in Figure S13 for the DH-EW test alongside results assuming the generic σ_{lnVs}.

The results provided by this application highlight minor differences in the variability of the Toro randomized V_S profiles and their ability to generate sets of consistent site signatures. Indeed, compatibility with experimental site signatures is only slightly improved. From the TDCs, the dispersion misfit m_d ([0.016; 0.626], average 0.149) slightly decrease compared to the case of generic σ_{lnVs} ([0.015; 0.411], average 0.109). Additionally, the individual and the mean randomized TTFs are not majorly affected by the choice of σ_{lnVs} when compared with the pseudo-Experimental transfer function (pseudo-ETF). The cross-validation error estimator Q^2 is slightly increased from 0.721 to 0.742 in the site-specific case, and the Pearson's correlation coefficient r_P is increased from 0.309 to 0.481, both values below 0.6.

Table S8. Values of site-specific σ_{lnVs} for the DH-EW base-case V_S profile in the Grenoble site.

Layer	Parameter	DH-EW
1	$\sigma_{lnVs\ 1}$	0.16
2	$\sigma_{lnVs\ 2}$	0.05
3	$\sigma_{lnVs\ 3}$	0.08
4	$\sigma_{lnVs\ 4}$	0.06
5	$\sigma_{lnVs\ 5}$	0.10
6	$\sigma_{lnVs\ 6}$	0.05
7	$\sigma_{lnVs\ 7}$	0.06
8	$\sigma_{lnVs\ 8}$	0.06

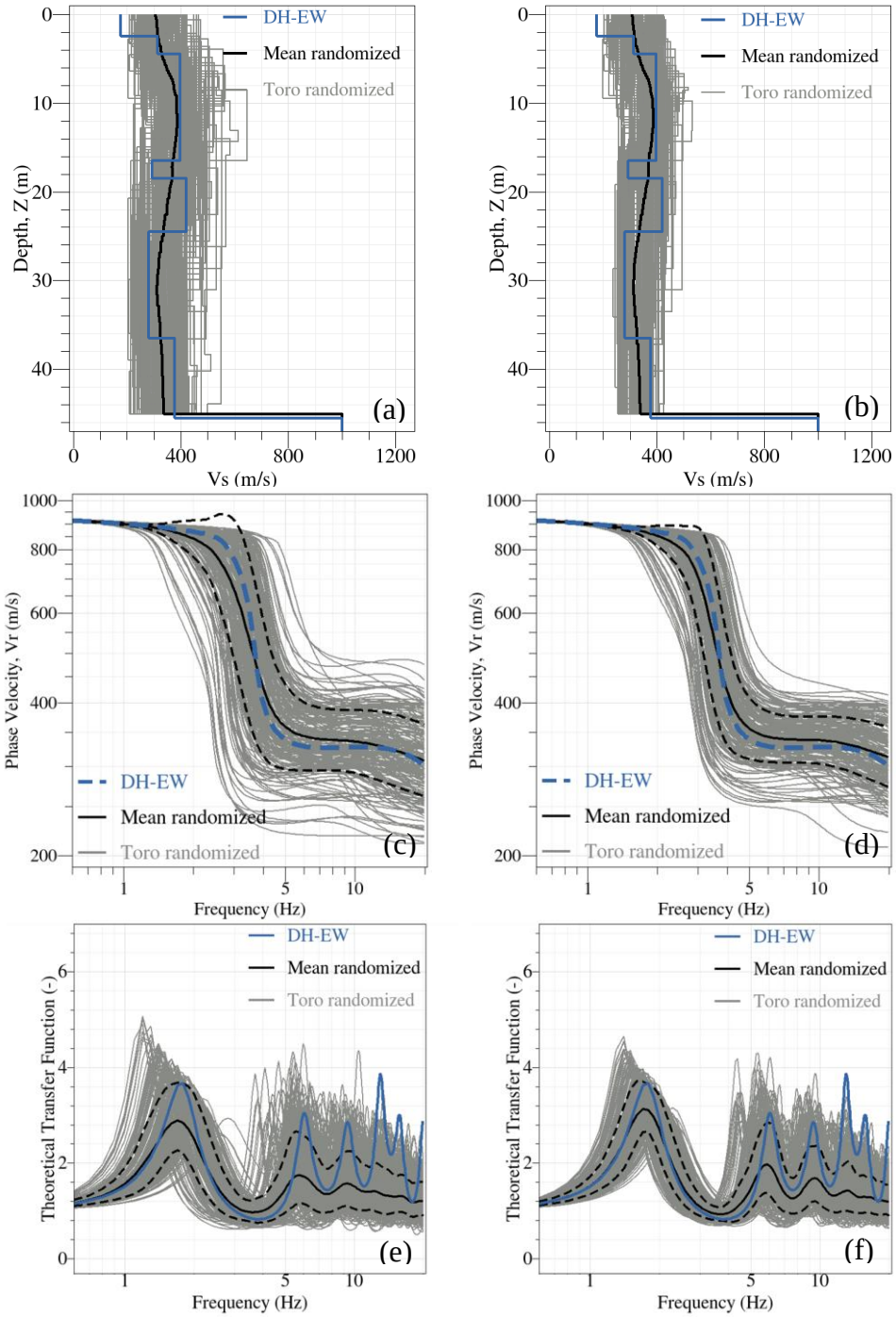

Fig. S13. Generated suites of 200 V_S profiles (a, b) following the Toro (1995) approach for DH-EW base-case V_S profile at Grenoble indicated in blue color, corresponding 200 sets of theoretical dispersion curves (c, d) and theoretical transfer functions (e, f) assuming generic σ_{lnVs} following the Toro (1995) model components (Stewart et al. 2014) (a, c, e) and site specific σ_{lnVs} from DH-EW V_S profile (b, d, f).

Appendix S6: Performance of V_S randomization approaches in terms of shear-wave cumulative travel time

The shear-wave cumulative travel time represents the time the S-waves take to travel from a certain depth, typically the bedrock interface, to the soil surface. It constitutes a fundamental quantity in site response studies since the travel time is directly related to the surface-wave dispersion and the site response itself (e.g. Brown et al. 2002; Passeri et al. 2020). The cumulative travel time is typically computed using Eq. S1 below.

$$tt_{S,z}(z) = \sum_{i=1}^{n} \left(\frac{h_i}{V_{S,i}} \right) \quad \text{(Eq. S1)}$$

In which z is the depth, n is the number of layers, h_i, and $V_{S,i}$ are the thickness and the S-wave velocity of layer i, respectively.

The S-wave travel times were computed using randomized V_S profiles from the non-stationary, stationary, and Toro's (1995) approaches to test their accuracy in reproducing measured S-wave travel times from different invasive tests. Here, the total travel time is assumed as the time it takes the wave to travel from the assigned soil-bedrock interface to the ground surface. Accordingly, cumulative travel times were computed for randomized V_S profiles across the three sites. However, we only show in this appendix the results for the Mirandola site since the Grenoble and Cadarache sites exhibited similar results.

The S-wave travel times from borehole measurements were determined for the six V_S profiles used at the Mirandola site. The values are indicated in Table S9.

Table S9. Cumulative S-wave travel time from six base-case V_S profiles in Mirandola site. Values are indicated in sec.

Site	PS-SL S-R1	PS-SL R1-R2	DH-EW	DH-NS	CH1	CH2
Mirandola	0.4000	0.4033	0.4013	0.3618	0.3931	0.3567

Computed travel times using the Non-Stationary, Stationary, and Toro randomized profiles are plotted in Figure S14 for the Mirandola site alongside the borehole travel times. Non-Stationary travel times converge with low scatter around the borehole travel times, while the Stationary and Toro travel times display systematically higher scatter.

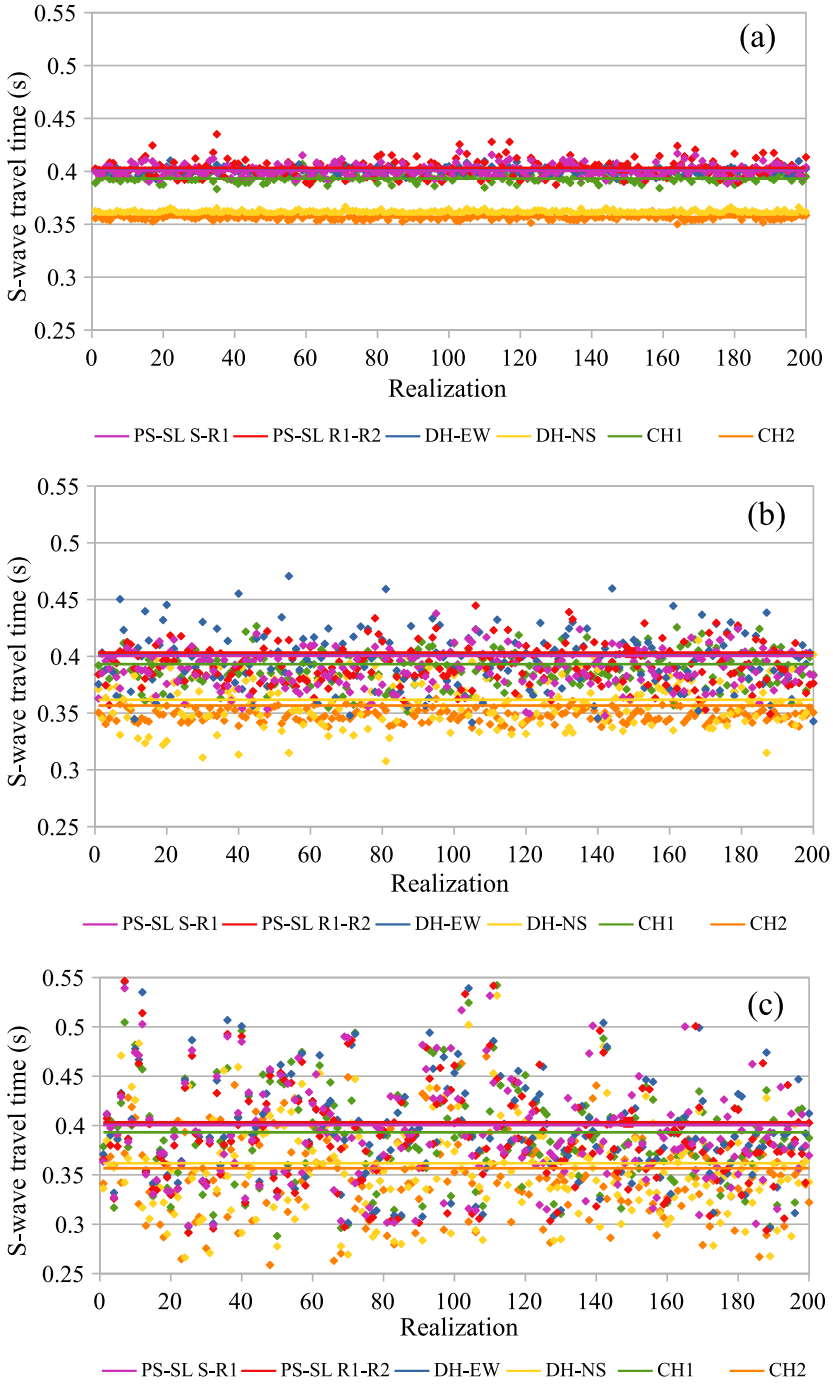

Fig. S14. Cumulative S-wave travel times computed from the non-stationary (a), stationary (b) and Toro's (1995) (c) randomized profiles for six base-case V_S profiles at Mirandola. Also plotted are the pseudo-experimental travel times computed from the borehole base-case V_S profiles at Mirandola site (continuous lines).

References

Brown, L. T., D. M. Boore, and K. H. Stokoe. 2002. "Comparison of shear-wave slowness profiles at 10 strong-motion sites from noninvasive SASW measurements and measurements made in boreholes." *Bull. Seismol. Soc. Am*. 92, 3116-3133.

Passeri, F., S. Foti, and A. Rodriguez-Marek. 2020. "A new geostatistical model for shear wave velocity profiles." *Soil Dyn. Earthquake Eng*. 136: 106247. https://doi.org/10.1016/j.soildyn.2020.106247.

Rathje, E. M., A. R. Kottke, and W. L. Trent. 2010. "Influence of input motion and site property variabilities on seismic site response analysis." *J. Geotech. Geoenviron. Eng.* 136(4), 607-19. https://doi.org/10.1061/(ASCE)GT.1943-5606.0000255.

Stewart J., K. Afshari, and Y. Hashash. 2014. *Guidelines for performing hazard-consistent one-dimensional ground response analysis for ground motion prediction*. Berkely, California: Pacific Earthquake Engineering Research Center.

Teague, D. P., B. R. Cox, and E. M. Rathje. 2018. "Measured vs. predicted site response at the Garner Valley Downhole Array considering shear wave velocity uncertainty from borehole and surface wave methods." *Soil Dyn. Earthquake Eng*. 113, 339–355.

Toro, G. 1995. *Probabilistic models of the site velocity profiles for generic and site-specific ground-motion amplification studies*. Technical Rep. 779574. New York: Brookhaven National Laboratory.

Toro, G. 2022. "Uncertainty in Shear-Wave Velocity Profiles." J. Seismol. 26, 713–730.